geosciences

MDPI

Article

Post-Collisional Cu-Au Porphyry and Associated Epithermal Mineralisation in the Eastern Mount Isa Block: A New Exploration Paradigm for NW Queensland

Kenneth D. Collerson [1,*] and David Wilson [2]

[1] School of the Environment, University of Queensland, St. Lucia, QLD 4072, Australia
[2] Transition Resources Limited, P.O. Box 78, San Remo, VIC 3925, Australia; david.wilson@transitionresources.com.au
* Correspondence: k.collerson@uq.edu.au

Abstract

Post-collisional Cu-Au-Ni-Co-Pt-Pd-Sc porphyry [Duck Creek porphyry system (DCPS)] with overlying Au-Te-Bi-W-HRE epithermal mineralisation [Highway epithermal system (HES)] has been discovered in the core of the Mitakoodi anticline, southwest of Cloncurry. Xenotime and monazite geochronology indicate mineralisation occurred between ~1490 and 1530 Ma. Host rock lithologies show widespread potassic and/or propylitic to phyllic alteration. Paragenesis of porphyry sulphides indicates early crystallisation of pyrite, followed by chalcopyrite, with bornite forming by hydrothermal alteration of chalcopyrite. Cu sulphides also show the effect of supergene oxidation alteration with rims of covellite, digenite and chalcocite. Redox conditions deduced from the V/Sc systematics indicate that the DCPS contains both highly oxidised (typical of porphyries) and reduced lithologies, typical of plume-generated tholeiitic and alkaline suites. Ni/Te and Cu/Te systematics plot within the fields defined by epithermal and porphyry deposits. Duck Creek chalcophile and highly siderophile element (Cu, MgO and Pd) systematics resemble data from porphyry mineral systems, at Cadia, Bingham Canyon, Grasberg, Skouries, Kalmakyr, Elaisite, Assarel and Medet. SAM geophysical inversion models suggest the presence of an extensive porphyry system below the HES. A progressive increase in molar Cu/Au ratios with depth from the HES to the DCPS supports this conclusion. Three metal sources contributed to the linked DCPS-HES viz., tholeiitic ferrogabbro, potassic ultramafic to mafic system and an Fe and Ca-rich alkaline system. The latter two imparted non-crustal superchondritic Nb/Ta ratios that are characteristic of many deposits in the eastern Mount Isa Block. The associated tholeiite and alkaline magmatism reflect mantle plume upwelling through a palaeo-slab window that had accreted below the eastern flank of the North Australian craton following west-verging collision by the Numil Terrane. Discovery of this linked mineral system provides a new paradigm for mineral exploration in the region.

Keywords: post-collisional porphyry; epithermal Au; North Australian craton; tholeiite and alkaline magmatism; superchondritic Nb/Ta ratios; slab window; exploration paradigm

Check for updates

Academic Editor: Olivier Lacombe

Received: 22 October 2025
Revised: 15 January 2026
Accepted: 16 January 2026
Published: 20 January 2026

Copyright: © 2026 by the authors. Licensee MDPI, Basel, Switzerland. This article is an open access article distributed under the terms and conditions of the Creative Commons Attribution (CC BY) license.

1. Introduction

Supply chain models indicate that during the next two decades, the demand for copper will exceed the total tonnage that has ever been mined throughout earth's history. This supply deficit is exacerbated by reduced production from major mines in Chile, Peru and Indonesia, a situation that has been compounded by a dearth of discoveries and by a

reduction in the size and grade of these deposits. These factors provide the rationale for exploration and discovery of new copper-rich systems in geopolitically safe jurisdictions. Cu-Au-bearing porphyry deposits are attractive exploration targets because, although they have low copper and gold grades, e.g., 0.5 to 1.5 wt.% Cu and 0.1 to 1.5 g/t Au, they are high tonnage systems, ranging from 10^6 to 10^9 tonnes [1,2].

Porphyry deposits occur in continental crust above subduction zones, where oceanic slabs release volatiles during dehydration, metasomatizing the overlying mantle wedge, facilitating partial melting and forming water-rich, metal-bearing oxidised juvenile mafic to felsic magmas [3–5]. However, porphyry deposits also occur in post-subduction continental collision zones associated with less hydrous magmas [6,7]. Metals are derived from several sources [2,8–10]. Copper is largely derived from hydrated subducted oceanic lithosphere and is introduced into the overlying mantle wedge by hydrous fluids. Metals are also derived from alkaline and tholeiitic plume magmas that enter the mantle wedge via slab tears, some of which may be "fossil" tears [8,10]. Porphyry systems containing a significant plume component are also generally enriched in Au and PGEs [11–16].

In water-rich sulphate-bearing oxidised magmas that generate porphyry Cu-Au deposits [17], sulphur controls the behaviour of Cu and other chalcophile elements, due to the high partition coefficients that exist between these elements in sulphides and silicate melts. Cu-rich sulphides in parental magmas are destroyed by oxidation increasing the chalcophile element concentration of the resulting sulphur-undersaturated magmas [18,19]. In these sulphide undersaturated magmas, Cu and Au both behave like incompatible elements [17], enabling chalcophile element concentrations to increase in evolving sulphate-bearing magmas. The precipitation of metals in porphyry systems is finally driven by sulphate reduction, crystallisation of magnetite, decreasing pH and degassing of oxidised gases [20]. Elements liberated from sulphides by sulphate reduction are scavenged by aqueous fluids. These fluids transport metals to shallower depths, into epithermal systems above the porphyry stockwork mineralisation [21]. Such epithermal vein and breccia precious metal-rich systems form from silica- and bicarbonate-rich hot springs at palaeo-depths of less than 1 km [22] forming a distinctive array of textures that are valuable exploration vectors [23].

Porphyry deposits are mainly preserved in less eroded Phanerozoic upper crust at depths between 2 and 4 km [23,24]. However, a few examples of Precambrian porphyry-epithermal mineralisation have been reported. For example, in the Archaean (2.83–2.82 Ga) Kolmozero–Voronya greenstone belt in the Kola Peninsula [25], in the Palaeo-to-Meso-Archean North Pilbara Terrane [26] and in Neoarchean crust at Boddington in the Southwest Yilgarn craton [27]. Porphyry mineralisation of Palaeoproterozoic age has also been described from the Tapajós Mineral Province in Amazonia, Brazil [28] and the Great Bear magmatic zone in Canada [29]. In fact, in the Great Bear magmatic zone, there is a continuum of deposit styles ranging between iron oxide copper gold IOCG mineralisation and arc-generated porphyry Cu-Au deposits [30]. Temporally and spatially associated IOCG and porphyry mineralisation of Mesoproterozoic age also occurs in the Gawler Craton, South Australia [31]. These provide a further example of the close spatial association between IOCG and porphyry deposits reported from Northern Chile [32]. According to Sillitoe [33], this close association could reflect variations in the level of exposure, with IOCG magnetite-Cu-Au deposits occurring at depth and oxidised porphyry style hematite Cu-Au mineralisation forming at shallower crustal levels.

In this paper, we report the discovery of Mesoproterozoic post-collisional porphyry and epithermal mineralisation in the eastern segment of the Mount Isa Block. It is preserved in a zone of low strain in the core of the Mitakoodi anticline, approximately 25 km southwest of Cloncurry. The mineral system is hosted by a suite of post-tectonic intru-

sive lithologies that include tholeiitic ferrogabbro, leuco-gabbronorite and anorthosite, as well as an alkalic suite that includes websterite, ultramafic lamprophyre, melilite-bearing gabbro and monzodiorite. These units crop out as roof pendants that intrude Marraba Volcanic meta-basalt, meta-andesite and tuffaceous units. Occurring above the porphyry mineralisation, at a higher palaeo-crustal level, are sheets of carbothermal lithologies and associated siliceous crackle breccias that preserve distinctive epithermal textures indicative of deposition from fumarolic CO_2-rich fluids. The epithermal vein and breccia system has a strike length of >20 km and is structurally controlled by axial plane shear zones of parasitic folds on the regional Mitakoodi anticline.

We review key lithogeochemical features of the Highway–Duck Creek mineral system using an extremely large petrological geochemical database. Using pivotal geochemical vectors that facilitated the discovery, we present an alternative metallogenic model for the Cloncurry region that better accommodates the geodynamic model for the tectonic evolution of the eastern flank of the North Australian Craton. Given the coherence of the lithogeochemical data, this model may be applicable to other deposits in the region, particularly to the so-called "within craton IOCG deposits" that have recently been classified as "intracratonic copper-gold deposits" by Brauhart and Groves [34].

The Mount Isa block, also referred to as the NWMP (Figure 1), is spectacularly enriched in a wide range of metals, including the Tier 1 sediment-hosted Mount Isa copper deposit, and the Ernest Henry iron–oxide–copper–gold (IOCG) deposit [35,36]. However, since the discovery of the Ernest Henry deposit more than 30 years ago, the region remains remarkably underexplored, and few significant new discoveries have been made. In view of the significant metal endowment of the province, this limited exploration success is an enigma. It may reflect the fact that current exploration models do not fully accommodate the possible existence of different mineral systems. Alternatively, it may simply reflect the fact that "barren" magnetic targets have been drilled rather than "fertile" non-magnetic hydrothermally altered targets.

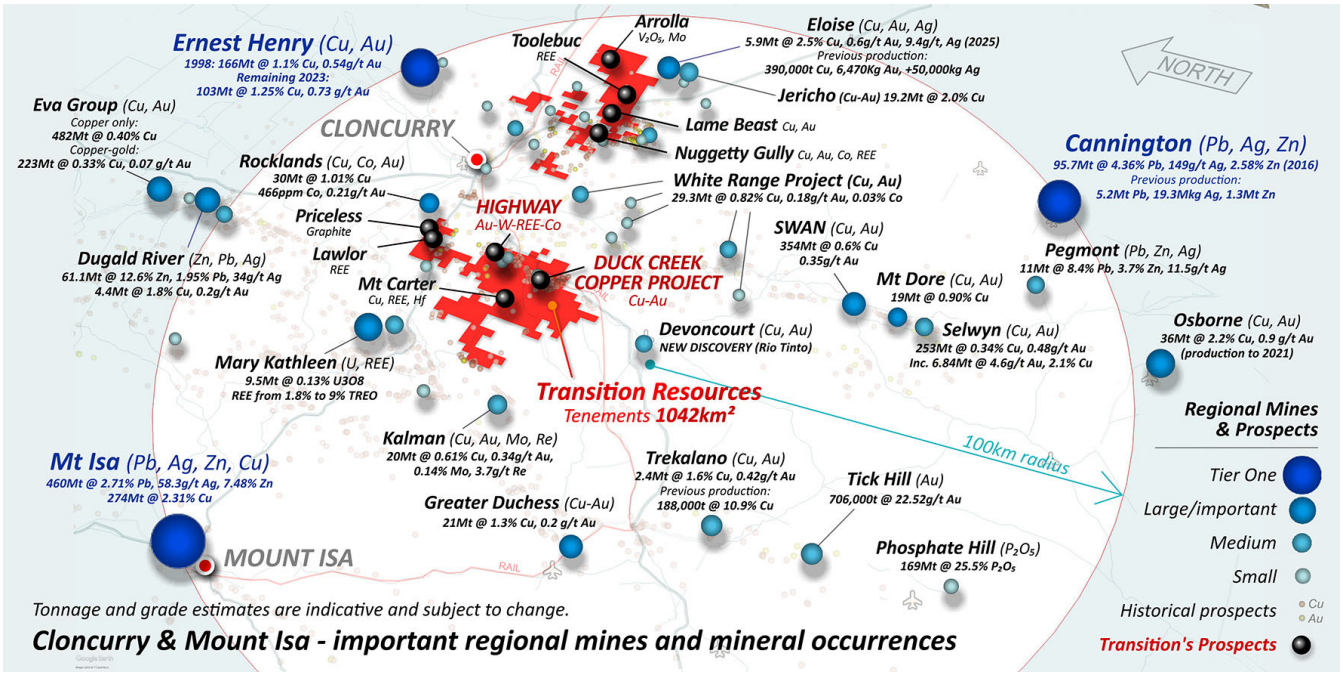


Figure 1. Map showing the location of the Highway–Duck Creek systems in relation to principle mineral deposits in the Northwest Minerals Province.

2. Geological Background

Exploration in the Cloncurry segment of the NWMP has largely focused on the post-Isan Orogeny Cu-Au-Co-REE-Re-Mo-U IOCG or iron sulphide-rich (ISCG) mineral systems. Metals are interpreted to have been derived either from a granitic source, such as the Williams–Naraku Batholith [37], or by mixing between magmatic fluids with basin brines [38–40]. Fluid inclusion studies and both stable and rare gas isotopes indicate that, although fluids largely display crustal isotopic signatures, there is a cryptic mantle signature [41]. However, neither the granitic nor the brine source accounts for the wide range of chalcophile (Ag, As, Bi, Cd, Cu, Hg, In, Pb, S, Sb, Se, Te, Tl, and Zn), siderophile (Co, Ni, Mo, W, Re, Os, Pt, Pd and Au) or lithophile (Sc, V, Cr, Y, Zr, Nb, REE, Th and U) abundances reported in these deposits. The multi-element association of Co-Ni-V-Sc-PGE with high Nb/Ta ratios reported in many Cloncurry deposits is clearly inconsistent with derivation from a crustal granitic source and requires the involvement of an ultramafic/mafic mantle-plume component.

Such an alkaline ultramafic suite occurs at Mount Cobalt, ~90 km south of Cloncurry [42]. These lithologies include olivine-bearing pyroxenites, with a superchondritic average Nb/Ta ratio of 25. As discussed later, elevated Nb/Ta ratios are clearly inconsistent with a crustal metal source, indicating Nb-Ta fractionation in either a mantle plume alkaline magmatic system [43], in metasomatised continental lithospheric mantle [44] or in deep arc eclogitic cumulates stored between 400 and 650 km in the transition zone [45]. The Mount Cobalt lithologies are extremely enriched in Co 10 wt.%, Ni 3117 ppm, Sc 278 ppm, Au 5 ppm, Pd 8 ppb, Pt 3.7 ppb, and they have significant concentrations of heavy rare earth elements, Dy up to 315 ppm and Tb up to 90 ppm. Thus, these lithologies provide direct evidence of a viable ultramafic source that accounts for the anomalous highly siderophile elements (Co, Ni, Mo, W, Re, Os, Pt, Pd) and Au in Cloncurry district mineral systems.

Furthermore, Ca-rich pyroxenites, melilite-bearing gabbroic lithologies and ultramafic lamprophyres with elevated superchondritic Nb/Ta ratios, up to 202, with an average of 48.6 (SD 29), are also present at the Elaine Dorothy copper prospect near Mary Kathleen uranium mine (Figure 1). They define a significant and continuous depth interval between 232 m and 871 m. Mafic lithologies with superchondritic Nb/Ta ratios are also present at Lawlor (Figure 2), ~10 km northeast of Highway, where values range up to 390 with an average of 54 (SD 81). These examples clearly provide additional evidence for the role of mafic alkaline magmatism in the area [46].

Such cryptic evidence for the role of plume magmatism within the eastern segment of the North Australian Craton, and the metal association of high-K calc-alkaline-hosted porphyry mineralisation in the eastern NWMP, is consistent with the inferred geodynamic evolution of the region. The eastern segment of the North Australian Craton is interpreted to be an early Proterozoic convergent Andean margin that developed above a west-dipping subduction zone [47]. This interpretation was subsequently confirmed by reflection seismology, with the identification of a prominent west-dipping feature, the Gidyea Suture, that extended below the Mount Isa Block that juxtaposed the outboard suspect Numil terrane with the North Australian Craton [48,49]. Thus, the Mesoproterozoic metallogenic endowment of the eastern NWMP appears to reflect the geodynamic interplay between subduction zone magmatism, back arc basin rift magmatism, slab tear facilitated tholeiitic and alkaline plume magmatism, collisional orogenesis and finally crustal anatectic magmatism that produced the regionally widely distributed alkaline and peraluminous Williams Naraku Batholith intrusions.

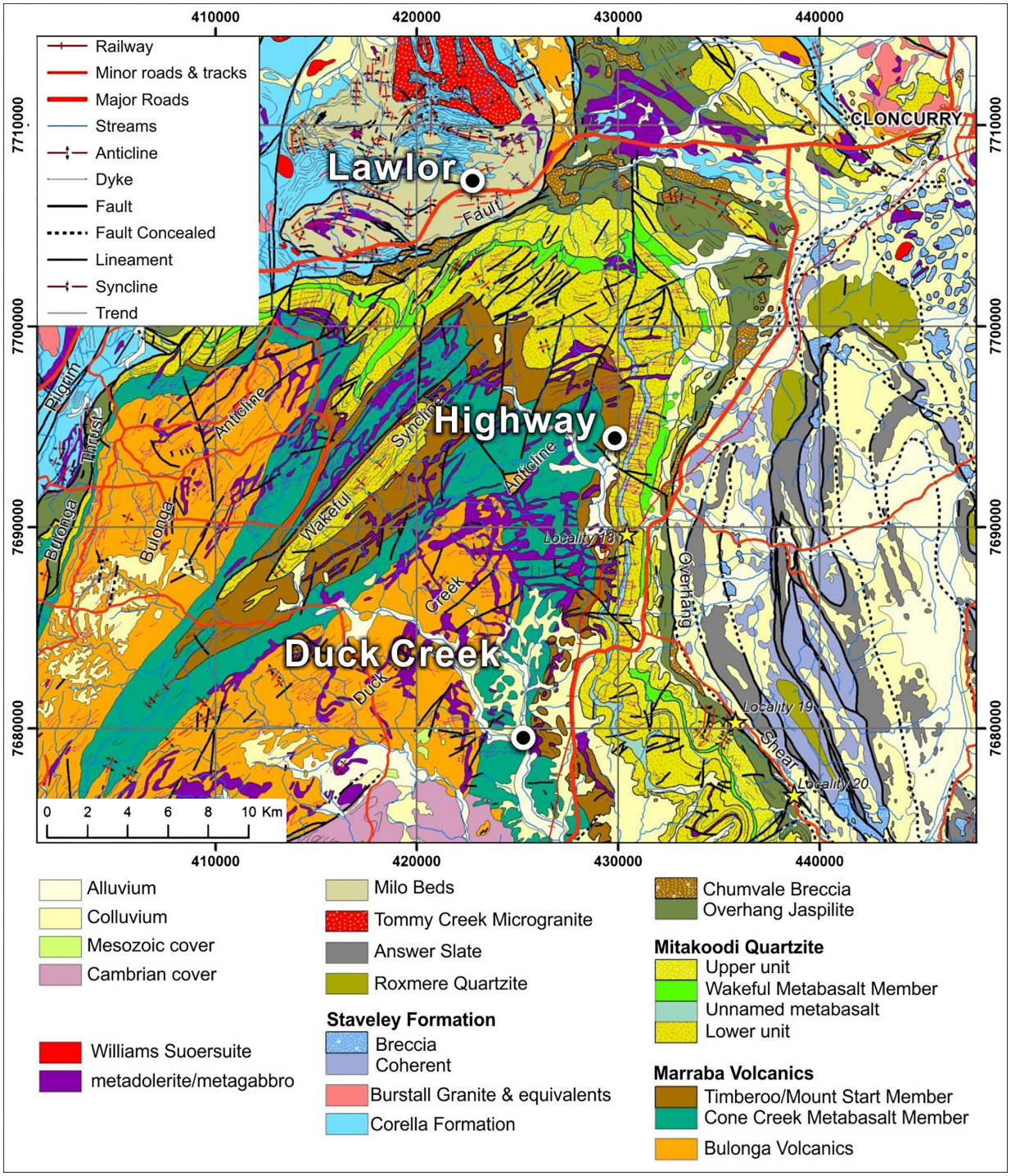


Figure 2. Geological map of the Mitakoodi anticline showing locations of the Highway, Duck Creek and Lawler prospects.

The involvement of Mesoproterozoic intraplate tholeiitic and alkaline plume magmatism in the NWMP is consistent with the geodynamic model that explains the breakup of the Columbia supercontinent, when the Paleo-Australian components of Columbia, i.e., the Gawler, Curnamona and North Australian Cratons traversed an upwelling mantle plume [50,51]. The eastern margin of the North Australian Craton in the Cloncurry area is a collisional orogenic belt, comprising an accreted collage of subduction-generated Palaeoproterozoic crust and telescoped back arc basins [36,52]. As collisional orogens are commonly underlain by slab tears [53,54], these tears provide a window for penetration

by an upwelling plume into either the mantle wedge or the sub-continental lithospheric mantle. The slab tear window most likely accreted to the base of the sub-continental lithospheric mantle, where it provided a conduit for ingress by upwelling plume magmas. Slab tears are a common feature of continent–continent collisional environments [54]. Metals in Mesoproterozoic NWMP deposits are interpreted to have been derived from two sources: Cu from altered subducted oceanic crust that was transported via hydrous fluids into the mantle wedge, and Cu, Au and platinum group elements introduced into continental lithosphere by tholeiitic and alkalic plume [55,56].

2.1. The Highway–Duck Creek Mineral System

Epithermal Au-Te-W-REE mineralisation, and the underlying porphyry Cu-Au-Co-Ni-Sc system, discovered southwest of Cloncurry (Figures 1 and 2), is a greenfield discovery, as there is no evidence in the field to indicate any previous mining activity in the area. Although the area contains a myriad of historic supergene copper workings, it had been overlooked for modern exploration for almost 100 years. The discovery was made using p-XRF analyses that showed elevated tungsten (W), gold (Au), and yttrium (Y) in silica-rich breccia that exhibited epithermal quartz textures. The name "Highway" was coined to acknowledge the anomalously ***high*** concentrations of ***W***, ***Au*** and ***Y*** in these breccias.

The silicic breccias and associated carbothermal veins, which contain elevated Au and tellurium (Te), have been traced for more than 20 km along the eastern limb of the Mitakoodi Anticline [57,58] (Figure 2). They are interpreted to have crystallised from boiling silica and CO_2—rich hydrothermal and carbothermal fluids at shallow crustal depths. These fluids accessed the axial plane shear zones of parasitic folds around the Mitakoodi anticline, where they precipitated.

The Duck Creek porphyry system occurs at a deeper level of crustal exposure in the core of the Mitakoodi Anticline, west of the Highway epithermal mineralisation. Lithogeochemical data for drill core indicate that mineralisation occurs in a post-tectonic potassic suite that includes olivine websterite, pyroxenite, gabbro, leucogabbro, anorthosite and monzodiorite and monzonites. In view of the common association between potassic magmatism and large, high-grade Cu-Au porphyry deposits, recognition of the involvement of post-tectonic potassic magmatism in the eastern NWMP has important implications for the resource potential of the Highway–Duck Creek discovery. The Highway–Duck Creek epithermal-porphyry mineralisation post-dates the ~1650 Ma thermotectonism in the Mount Isa Block.

The discovery was facilitated through the application of a new exploration model for the Cloncurry region based on results reported by Collerson in [42]. This model specifically addressed apparent deficiencies with the IOCG model that specifically focused on the role played by post-tectonic Williams Batholith granitoids, whose felsic compositions failed to explain the distinctive element association, viz., Cu-Au-Ni-Co-Pt-Pd-Sc (±HREE + Y) and the superchondritic Nb/Ta recorded in the Highway–Duck Creek mineralisation. The model provided an alternative explanation for the spatial association and source of metals in iron–oxide–copper–gold (IOCG) and iron–sulphide–copper–gold (ISCG) mineralisation in the Cloncurry area cf. Skirrow [59], which have recently been assigned to members of a new clan of intracratonic ore deposits by Brauhart and Groves [34]. By accommodating spatial and geochemical relationships of mineralisation within a coherent narrative that is consistent with models for the geodynamic evolution of the eastern margin of the North Australian Craton, the new model clearly provides a plausible exploration basis for future discoveries.

2.2. Geological Setting of the Mitakoodi Domain

The megascopic scale Mitakoodi anticline (Figure 2) [57,58] and an associated west-verging thrust system formed during the Isan Orogeny at ~1650 Ma [57,58,60,61]. The core of the Mitakoodi anticline is a region of low finite strain that preserves a varied sequence of Marraba Volcanic lithologies, including the Bulonga Volcanics, the Cone Creek and the Timberoo Members. The Bulonga Volcanics are conformably overlain by interbedded mafic volcanics, fine clastic units of Marraba Volcanics and by a thick (up to 2000 m) succession of quartzo-feldspar arenite, termed the Mitakoodi Quartzite. The Mitakoodi Quartzite contains minor interbedded lenses of siltstone and metabasalt, as well as a unit of thinly bedded tuff near the top of the sequence.

The top of the quartzite contains a unit of porphyritic rhyolite, which has been mapped for a strike length of >3 km. As rhyolite is a high viscosity magma that forms lava domes, not extensive flows, the rhyolite sequence is possibly better interpreted as a pyroclastic ignimbrite sheet or tuff. A U-Pb SHRIMP zircon age of 1755 ± 4 Ma for the "rhyolite" [58] is within error of the age of the felsic Bulonga volcanic unit dated by Neumann et al. [62] in the core of the Mitakoodi anticline. The entire package of lithologies that crop out in the Mitakoodi Culmination represents a previously unrecognised intraplate suite that was possibly deposited in a back-arc rift environment. Some mafic units are quite massive and most likely represent high-level ultramafic to mafic plutonic bodies.

The Mitakoodi Domain was subsequently intruded by phases of the Wimberu Granite member of the Eureka Supersuite of plutons within the Williams Batholith. The Wimberu Granite yields LA-ICP-MS zircon U/Pb ages of 1518 ± 4 and 1483 ± 4 Ma [63]. This younger Williams–Naraku Batholith magmatism between ~1530 and 1490 Ma resulted in the formation of a complex suite of granitoids ranging in composition from dioritic through monzonitic, syenitic to granitic compositions with A-type geochemical signatures. Highway lithologies intrude regionally extensive rhyodacitic and rhyolitic lithologies of the 1750 ± 4 Ma Bulonga Volcanics [62] in the core of the Mitakoodi anticlinorium (Figure 2). This has been confirmed by laser ablation U-Pb geochronological data for xenotime and monazite from the Highway Breccia, which yield ages of ~1530 Ma and ~1490 Ma, respectively.

2.3. Field Relationships and Petrology

The Highway system is characterised by dominantly mono-lithologic quartz crackle breccias containing angular clasts that are cemented in a metal-rich matrix (Figure 3a–e). They contain chalcedonic siliceous vuggy veins, with characteristic epithermal textures, e.g., comb-textured microcrystalline quartz, crustiform–colloform banded quartz and lattice textures (Figure 3d,f). The distinctive epithermal lattice texture in Figure 3f is interpreted to have formed by quartz replacing earlier deposited calcite in a hydrothermal system. Such textures are characteristic of low-sulphidation, epithermal environments, where boiling carbonate-rich hydrothermal fluids culminated in the release of CO_2. Field and petrographic observations indicate that the breccias, the epithermal-textured siliceous veins and the carbothermal veins and carbothermal lithologies (Figure 3g) were deposited from a carbonate-rich hot spring (travertine), some of which contain chalcedonic clasts (Figure 3h).

In thin section, the epithermal lithologies exhibit very distinctive textures (Figures 4 and 5). Examples include interlayered quartz comb texture in a carbonate matrix (Figures 4a and 7b), a vein of epithermal quartz cutting propylitically altered gabbro (Figure 4c,d), a fine grained siliceous brecciated unit cemented by veins of epithermal quartz (Figures 4e and 7f), cross-cutting carbothermal and siliceous epithermal veins that indicate the impact of several hydrothermal events in the area (Figure 4g,h) and siliceous comb textures (Figure 4i). Also

shown is a reflected light image of a Highway epithermal lithology containing multiple grains of gold.

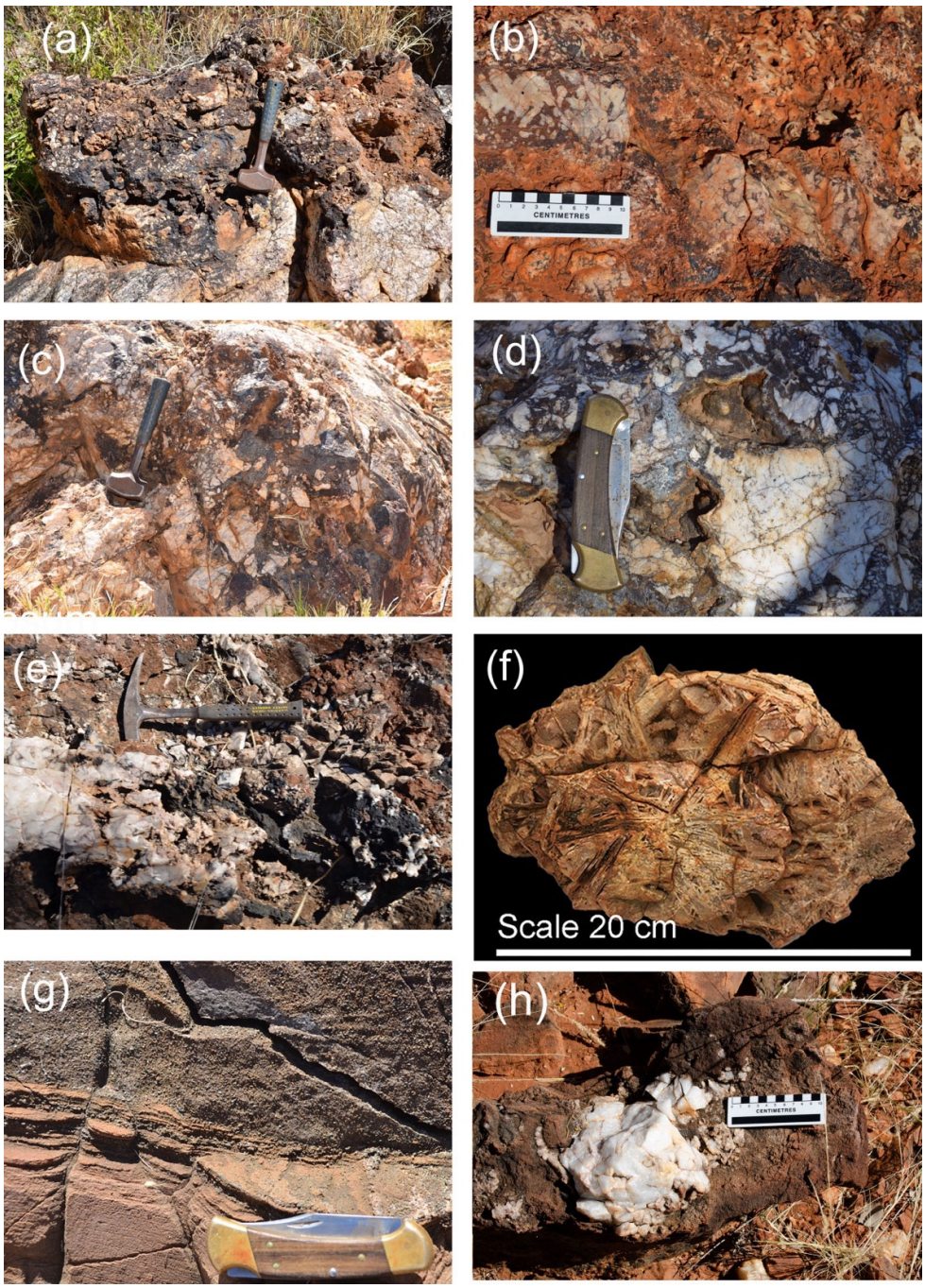


Figure 3. Highway epithermal lithological variation: (**a**–**e**,**h**) siliceous breccias showing embayed clasts of milky quartz, (**f**) rhombohedral carbonate pseudomorphed by epithermal silica, (**g**) carbothermal sinter and (**h**) embayed siliceous clast in a carbothermal matrix.

Photomicrographs of typical Highway carbonate- and quartz-bearing carbothermal lithologies are shown in Figure 5. Xenomorphic and idiomorphic grains of quartz typically exhibit slightly embayed grain boundaries that reflect the effect of acid (HF?) corrosion (Figure 5a–d,g–i). Some of the carbothermal units are tourmaline-bearing (Figure 5e,f), indicating that boron was an important component in the hydrothermal fluids.

Boron is a highly fluid-mobile vector of magmatic–hydrothermal systems, a common component of porphyry-related systems and related epithermal deposits, and a vector

indicating the presence of a deeper porphyry copper deposit [64]. Figure 5j shows a back-scattered electron image of pyrite containing inclusions of gold and bismuth telluride. Gold and bismuth tellurides are key components of some epithermal gold deposits, forming from hydrothermal fluids and often associated with alkaline or sub-alkaline magmatism [65].

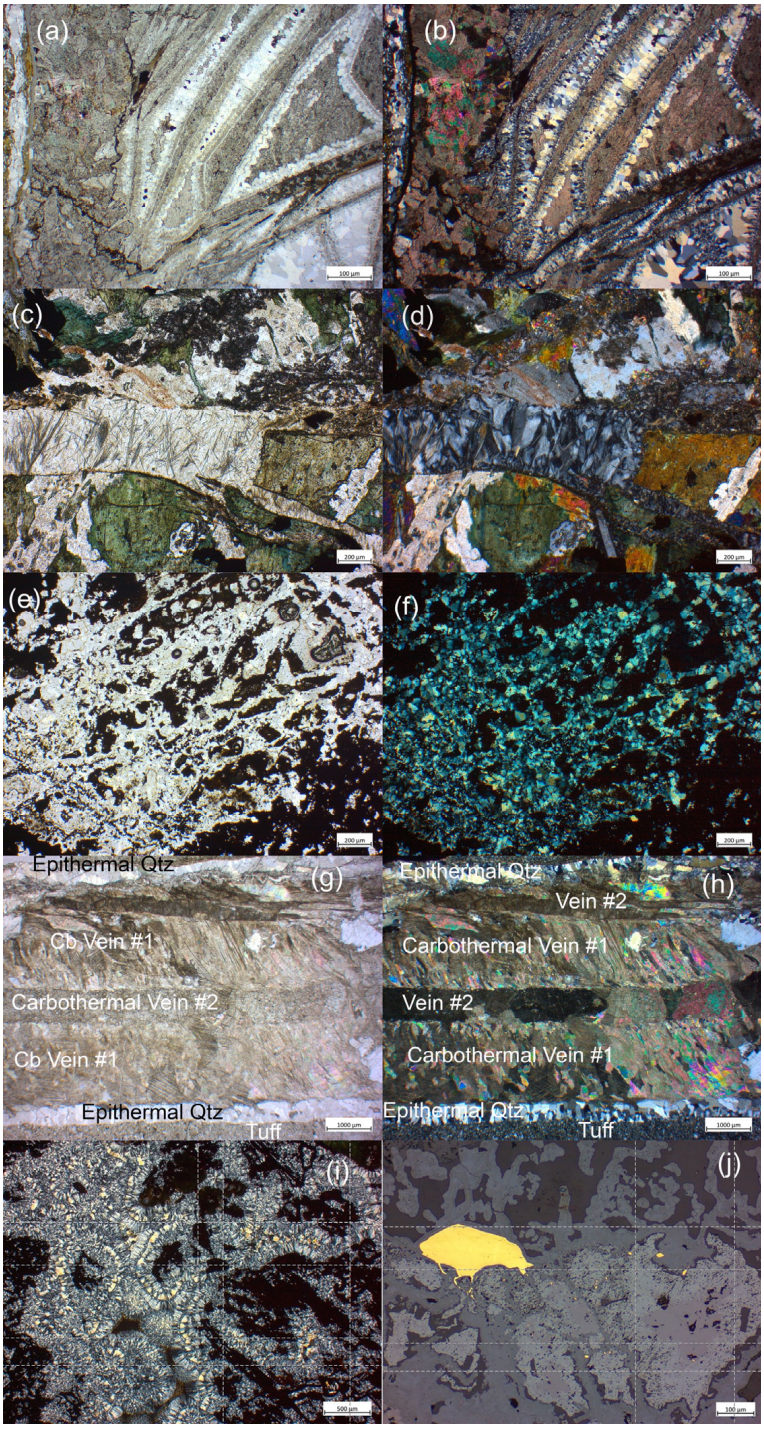


Figure 4. Photomicrographs of epithermal textures: (**a**,**b**) interlayered quartz comb texture in a carbonate matrix in plane and cross-polarised light, (**c**,**d**) vein of epithermal quartz cutting gabbro that exhibits propylitic alteration in plane and cross-polarised light, (**e**,**f**) fine-grained siliceous brecciated unit cemented by veins of epithermal quartz in plane and cross-polarised light, (**g**,**h**) carbothermal and siliceous epithermal veins showing evidence of several hydrothermal events in plane and cross-polarised light, (**i**) classic epithermal siliceous comb textures in cross-polarised light, (**j**) reflected light image showing grains of gold in Highway epithermal lithology.

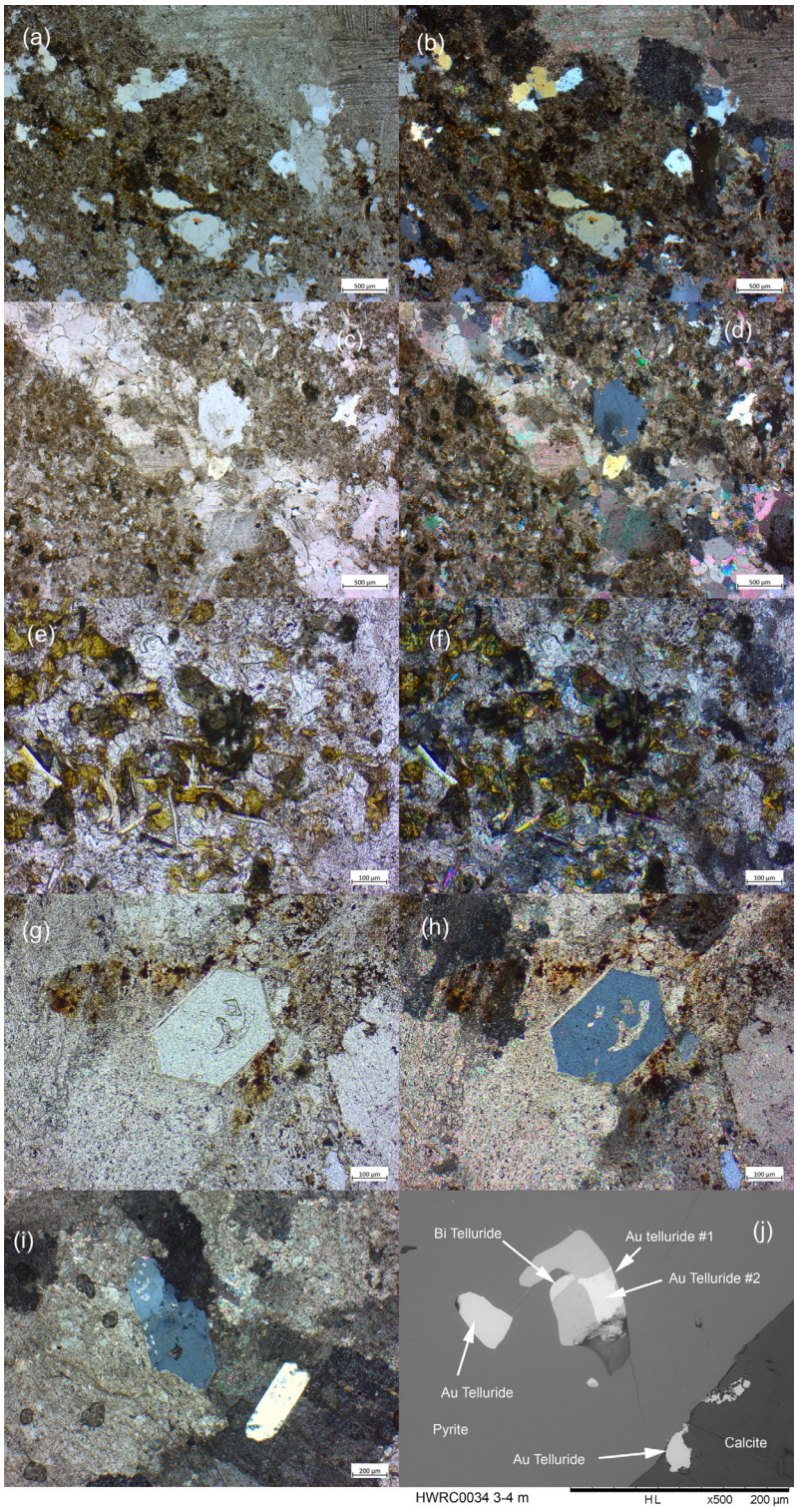


Figure 5. Photomicrographs of typical Highway epithermal lithologies in plane and cross-polarised light: (**a**–**d**,**g**–**i**) carbothermal lithologies with xenomorphic and idiomorphic grains of quartz that show embayed grain boundaries caused by acid (HF?) corrosion, (**e**,**f**) tourmaline-bearing carbothermal lithology, which shows the role of B in the fluid phase, (**j**) back-scattered electron image of Au and Bi tellurides in pyrite.

2.4. Duck Creek Mafic Intrusive Complex

Tholeiitic ferrogabbros, gabbronorites, leucogabbros and anorthosites are medium to fine-grained, with intergranular to subophitic textures. The absence of deformational

fabrics clearly indicates that the intrusions were emplaced after thermotectonism in the NWMP (Figure 6).

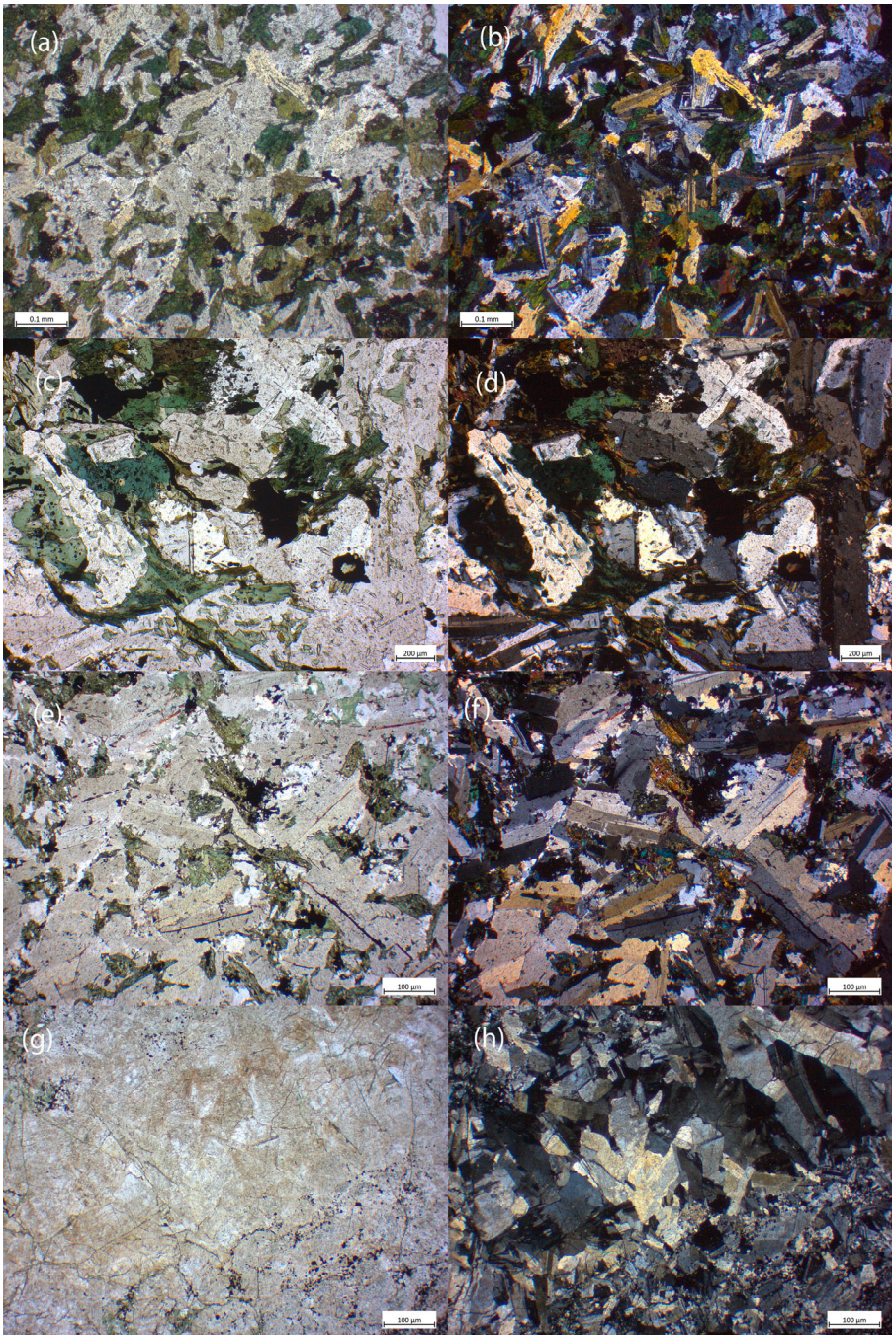


Figure 6. Photomicrographs of gabbro (**a**–**d**), leucogabbro (**e**,**f**) and anorthosite (**g**,**h**) from the tholeiitic ferro-mafic unit that intrudes the Bulonga Volcanics in plane and cross-polarised light showing intergranular and sub-ophitic textures. These are clearly undeformed and are therefore interpreted to be post-tectonic and therefore post-Isan orogeny.

The fine-grained size of these samples is interpreted to indicate that they represent the upper chilled margin of a much larger, deeper intrusive complex. This is supported by the fact that they crop out as roof pendants within the Marraba Volcanics (Figure 2). The intrusion contains lithologies that resemble lithologies in the plume-generated Nain Plutonic Suite, Labrador, Canada [66]. The lack of seismic anisotropy in the deep crust

below the eastern margin of the North Australian Craton [48,49] shows the extensive nature of this mafic intrusive complex.

2.5. Alteration in the Highway–Duck Creek Mineral System

Marraba volcanics host lithologies, and members of the later ferrogabbro to monzogabbro suite all show the effect of penecontemporaneous pervasive alteration (Figure 7).

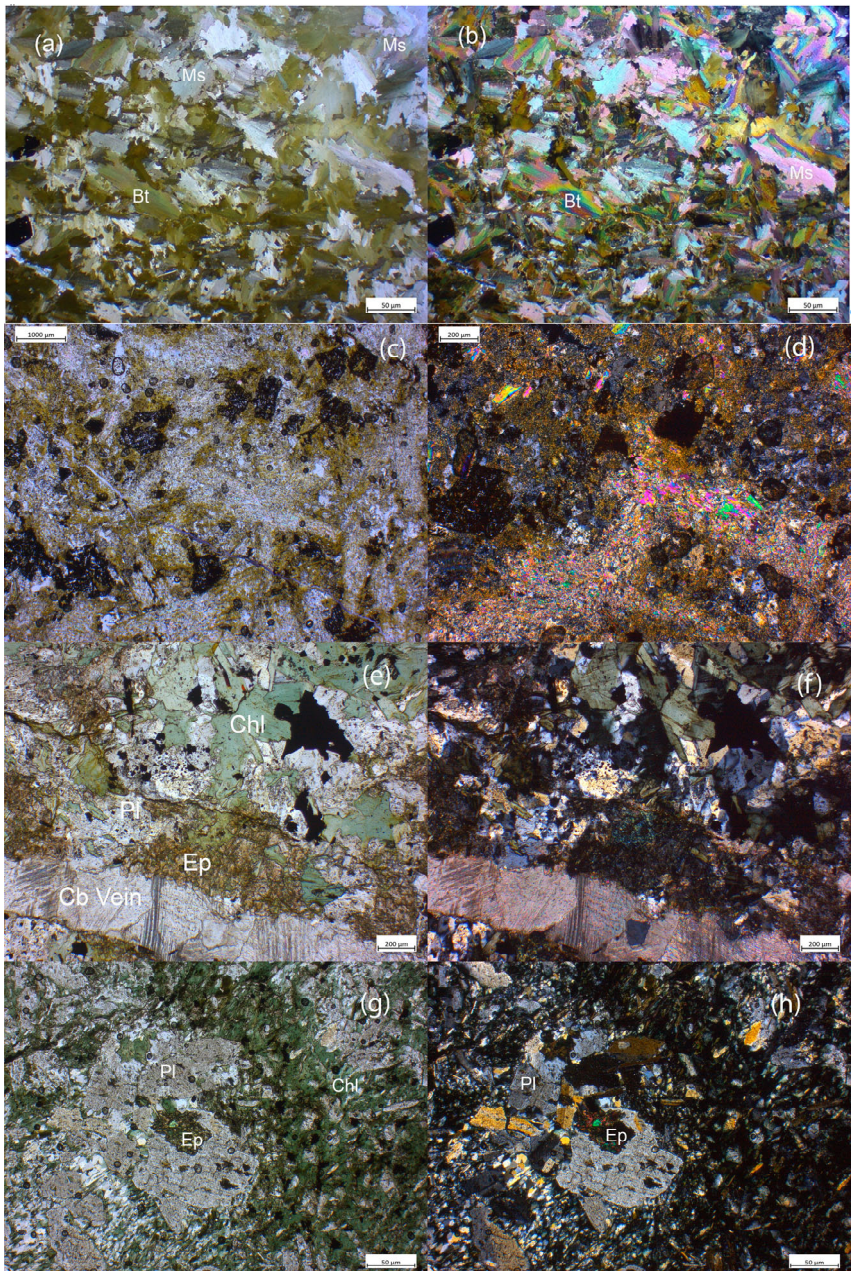


Figure 7. Photomicrographs in in-plane and cross-polarised light showing (**a**,**b**) phyllic alteration and (**c**–**h**) propylitic alteration.

The alteration assemblages overprint metamorphic microstructures in the Marraba volcanics and igneous textures in the ferrogabbro to monzogabbro suite. Typical alteration facies include the following:

(1) Phyllic alteration is shown by the presence of white mica (sericite) and quartz, together with chlorite, carbonate and tourmaline (Figure 7a,b). This alteration is caused by hydrolysis due to the interaction between high temperature, moderately acidic fluids

and host protoliths. The presence of carbonate and tourmaline indicates that the hydrothermal fluids were CO_2 and boron-bearing. Tourmaline is a common phase in both phyllic and propylitic alteration haloes associated with epithermal and porphyry Cu-Au mineral systems [67]. Carbonate is also a common phase in phyllic alteration haloes and indicates that the alteration fluids have near-neutral pHs [68].

(2) Propylitic alteration is shown by the presence of chlorite, epidote, carbonates (calcite), albite and pyrite, often replacing original ferromagnesian minerals like biotite and amphibole (Figure 7c–h). It is also a common feature along the margins of porphyry copper and associated epithermal precious metal deposits.

(3) Potassic alteration is shown by the presence of secondary biotite, K-feldspar (orthoclase) and sometimes muscovite or sericite. It forms by the reaction between protoliths of different compositions with hot (420–500 °C) metal-rich fluids. Potassic alteration is commonly associated with sulphide mineralisation, near the core of porphyry copper–gold systems.

3. Highway—Duck Creek Mineralisation

Figure 8 shows reflected light and back-scattered electron image examples of pyrite and Au telluride (Figure 8a), scheelite and wolframite (Figure 8b,c,f), gold mineralisation (Figure 8d,e), titanomagnetite and pyrite (Figure 8g) and titanomagnetite (Figure 8h,i) in Highway epithermal lithologies.

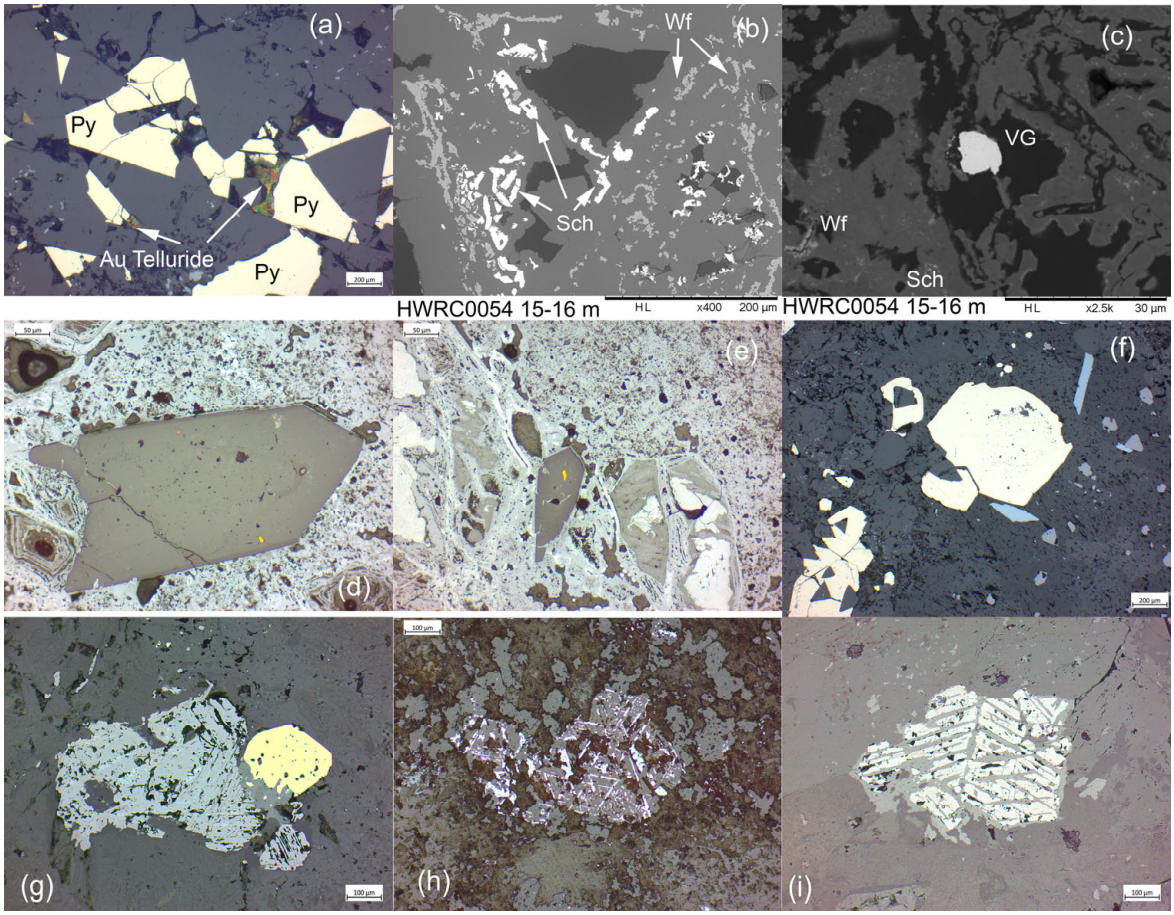


Figure 8. A selection of photomicrographs in reflected light and back-scattered electron images showing (**a**) pyrite and Au telluride, (**b**) scheelite and wolframite, (**c**) scheelite, wolframite and gold, (**d**,**e**) gold in quartz crystals, (**f**) pyrite and wolframite, (**g**) titanomagnetite and pyrite and (**h**,**i**) titanomagnetite in Highway epithermal lithologies.

Rare earth elements in the Highway epithermal system occur in monazite and xenotime. As these phases occur in cross-cutting veins (Figure 9), this mineralisation was clearly of hydrothermal origin.

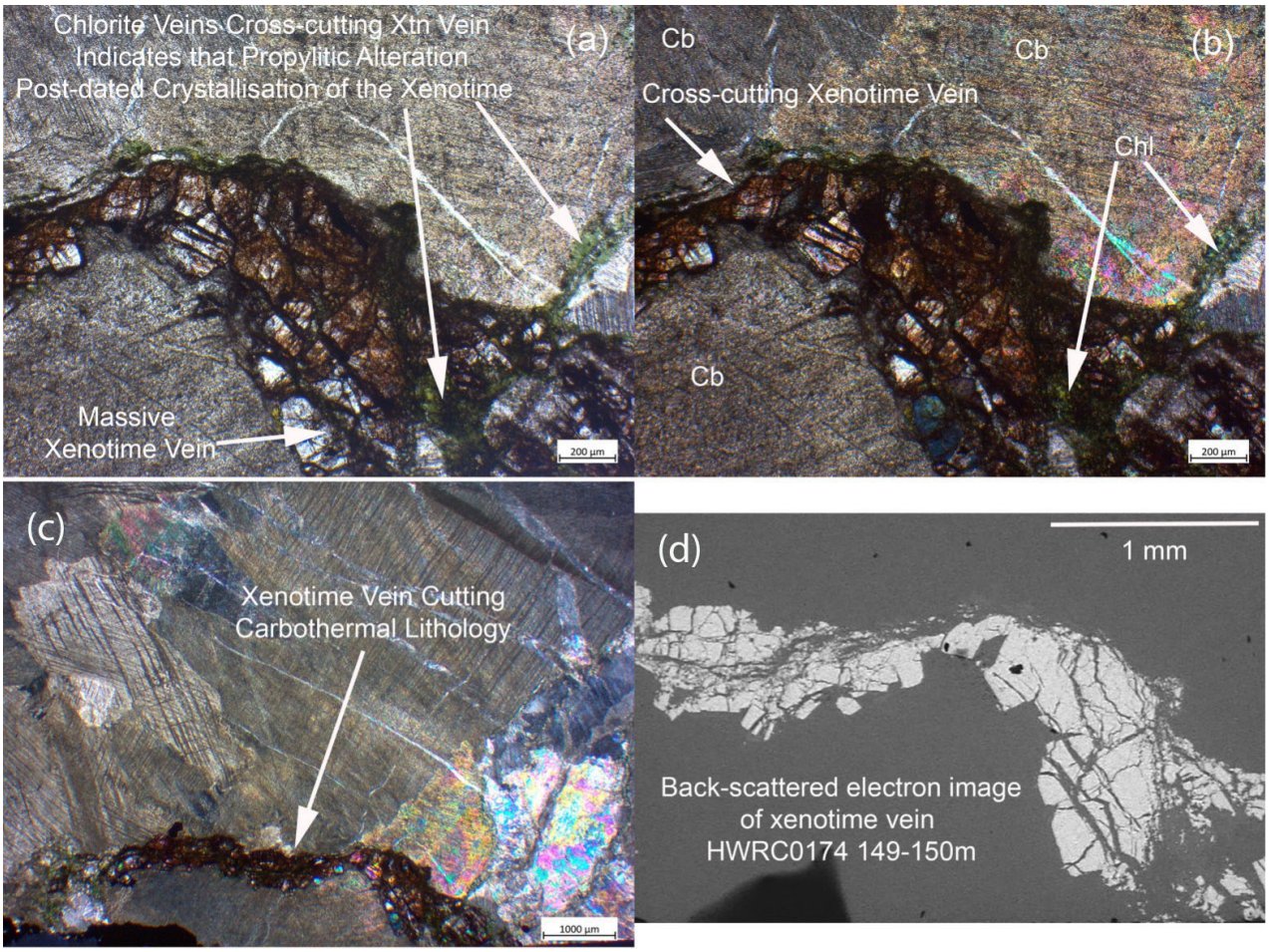


Figure 9. Carbothermal lithology showing details of a cross-cutting vein of xenotime in (**a**) plane polarised light, (**b**,**c**) cross-polarised light and (**d**) back-scattered electron image.

Textures and paragenetic relationships of Cu sulphides in the deeper Duck Creek mineral system are shown in Figure 10. Samples are mainly from the diamond drill core from the New Dollar deposit, which is located between Columbiad and Horseshoe (Figure 11).

Sulphide paragenetic relationships show early formed crystallisation of euhedral pyrite and then subsequent crystallisation of chalcopyrite (Figure 10a,e). In some samples, the early-formed pyrite is brecciated and cut by narrow veins of chalcopyrite. Chalcopyrite typically exhibits coronas of hydrothermal bornite, possibly formed by sulphidation of haematite [68,69] (Figure 10b,c). Supergene alteration of chalcopyrite is shown by formation of digenite and covellite (Figure 10d,f,g). Figure 10h shows pyrite pseudomorphs surrounded by chalcopyrite with rims of digenite New Dollar (19 m).

The presence of early euhedral pyrite and later chalcopyrite is a common paragenetic feature of many Cu-Au porphyry systems, e.g., Cadia in N.S.W. The presence of early formed euhedral pyrite in porphyries is interpreted to indicate that it crystallised from a hydrothermal fluid [70]. Bornite overgrowths on chalcopyrite are interpreted to have formed by hydrothermal alteration (Figure 10b–h). Bornite shows the pervasive effect of supergene replacement by digenite, covellite and chalcocite. The presence of abundant interstitial chalcopyrite in the ferro-gabbroic to monzogabbroic suite indicates a close relationship to the porphyry mineralising event.

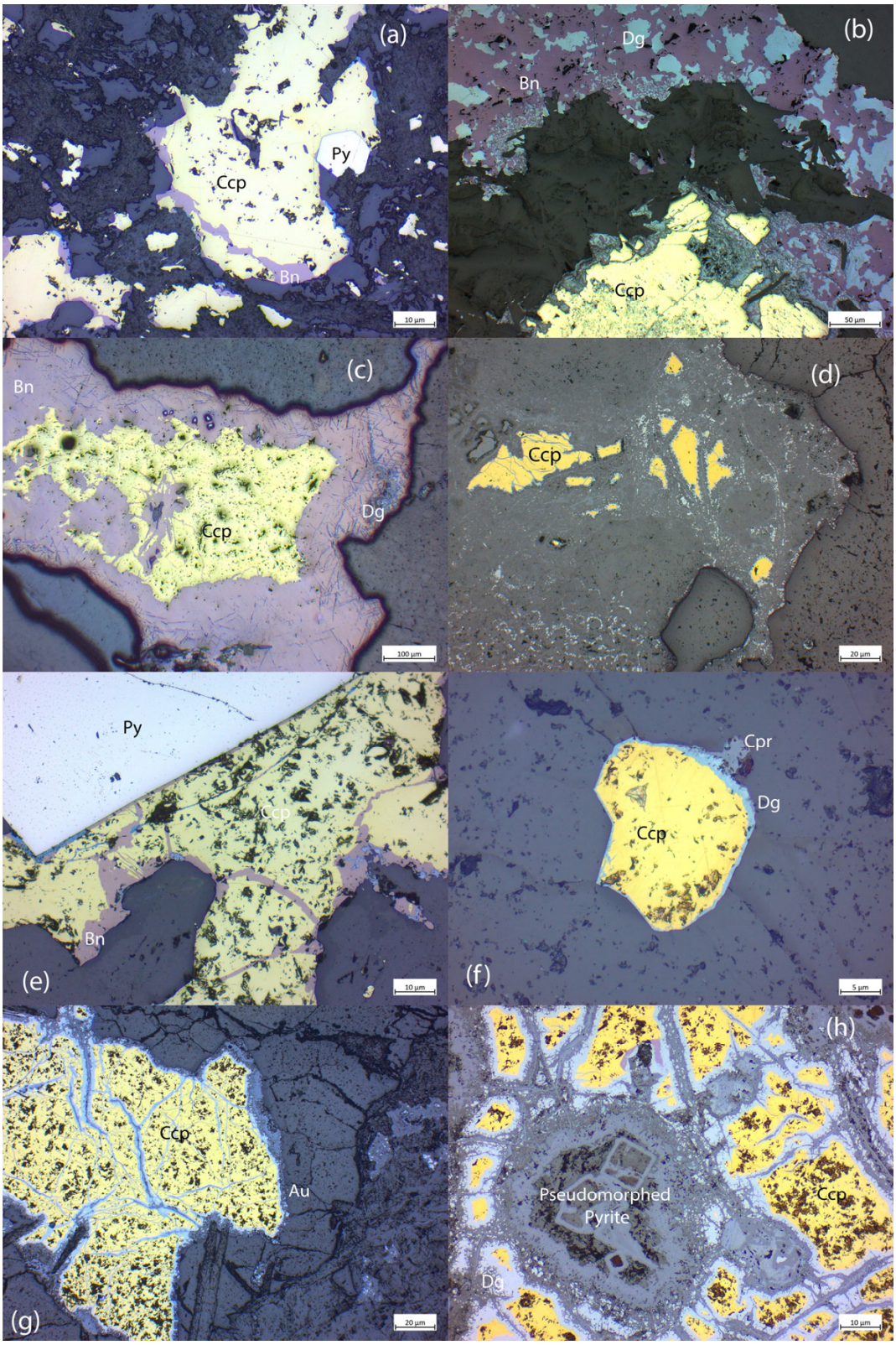


Figure 10. Photomicrographs of sulphides from the Duck Creek porphyry system in reflected light: (**a**) sulphide paragenetic relationship at Meteor (125 m) showing euhedral pyrite, overgrown by chalcopyrite and bornite, (**b**,**c**) chalcopyrite rimmed by digenite, bornite and covellite at New Dollar (85.3 m and 140 m), (**d**) chalcopyrite with narrow rims of digenite New Dollar (140 m), (**e**) euhedral crystal of pyrite with an overgrowth of chalcopyrite and rim of bornite produced by hydrothermal alteration, New Dollar (150 m), (**f**,**g**) chalcopyrite with coronas of digenite New Dollar (19 m), (**h**) pyrite pseudomorphs surrounded by chalcopyrite with rims of digenite New Dollar (19 m).

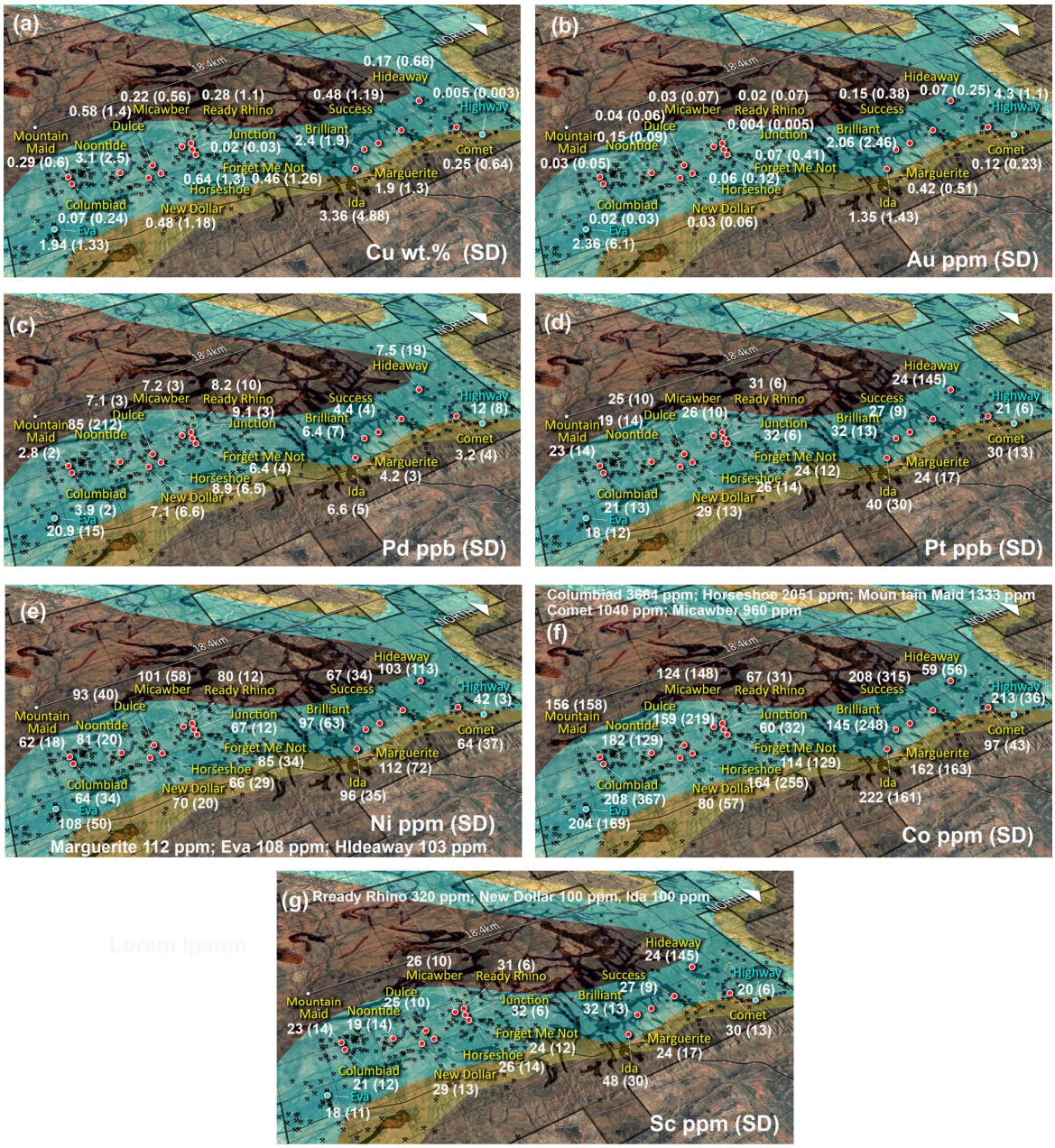


Figure 11. Maps showing the average and (SD) concentrations of (**a**) Cu wt.%, (**b**) Au (ppm), (**c**) Pd (ppb), (**d**) Pt (ppb), (**e**) Ni (ppm), (**f**) Co (ppm) and(**g**) Sc (ppm) in selected prospects (red dots) along an 18.4 km strike length within the Duck Creek porphyry system (pale green ornamentation) and the overlying Highway epithermal system (pale yellow ornamentation). Shown by the small dark dots are the myriad of small historic supergene mineralised deposits.

4. Materials and Methods

4.1. Materials

Samples from the Highway and Duck Creek were collected by KDC and by DW and geological staff employed by Transition Resources between 2018 and 2025.

4.2. Methods

The polished thin sections were prepared in the Queensland University of Technology lapidary facility. Petrographic studies were undertaken by KDC using a ZEISS Axio-scope 5 Polarising Reflected/Transmitted Light Petrographic Microscope in the School of the Environment, at the University of Queensland. Mineral identifications were confirmed

using a Hitachi TM3030 Scanning Electron Microscope (SEM) equipped with a Bruker Energy Dispersive Spectrometer (EDS) in the School of the Environment at the University of Queensland.

Analytical data reported and discussed in this paper were obtained using XRF, fusion ICPOES, fusion ICPMS and fire assay provided by Intertek, Perth and Townsville. Certified litho-geochemical standards were analysed with all sample submissions, and a full QA/QC assessment for accuracy was undertaken.

The data includes representative major and trace element analyses of lithological groups identified in rock chip and drill core from the Highway epithermal system (Table 1). These were selected from a data set of >33,287 analyses of rock chips and both RC and DD drilling at Highway.

Table 1. Partial major element analyses for variably altered lithologies from the Highway epithermal system.

	#1	#2	#3	#4	#5	#6	#7	#8	#9	#10	#11	#12
Number of Analyses	154	783	426	888	12	64	1045	722	47	435	15	163
SiO_2	51.71	52.86	53.49	50.51	59.84	58.37	60.69	61.91	57.35	58.02	73.87	70.66
TiO_2	0.40	0.81	0.64	1.55	0.47	0.67	0.59	0.49	0.44	0.23	0.30	0.26
Al_2O_3	12.74	11.89	12.39	11.63	13.49	12.19	13.72	13.20	9.46	5.28	4.75	7.44
Fe_2O_3	16.99	13.91	10.74	16.42	14.48	9.64	9.21	7.58	8.87	7.77	12.21	12.32
MnO	0.13	0.17	0.13	0.17	0.18	0.13	0.08	0.12	0.26	0.38	0.69	0.22
MgO	4.40	4.73	4.00	4.55	2.96	4.76	3.81	3.58	3.32	2.94	1.52	1.77
CaO	2.12	6.50	4.65	6.02	1.25	6.55	3.48	5.71	13.97	20.46	1.33	2.11
Na_2O	1.01	1.62	1.40	2.01	0.84	1.28	2.24	2.10	0.94	0.40	0.65	0.33
K_2O	2.23	2.27	2.37	1.38	3.18	3.25	3.01	2.15	2.24	1.37	1.56	1.73
P_2O_5	0.27	0.24	0.19	0.26	0.31	0.16	0.17	0.16	0.15	0.15	0.12	0.16
LOI	8.00	5.00	10.00	5.50	3.00	3.00	3.00	3.00	3.00	3.00	3.00	3.00
Total	100.0	100.0	100.0	100.0	100.0	100.0	100.0	100.0	100.0	100.0	100.0	100.0
Li	18.3	13.7	15.1	13.2	10.8	5.9	16.0	13.0	10.5	7.0	14.2	8.6
Sc	35	33	24	38	36	24	18	17	19	14	23	25
V	359	322	208	356	378	193	142	127	172	108	151	203
Cr	74	64	66	49	78	86	67	57	51	28	48	55
Co	126	73	57	78	75	40	34	28	60	237	229	170
Ni	55	47	42	41	50	48	42	37	37	38	44	43
Cu	53	94	73	413	30	39	35	29	34	86	38	22
Zn	26	21	28	37	22	26	25	12	31	12	10	21
Ga	22	21	19	22	26	19	20	20	16	11	9	14
Ge	1.33	1.27	1.44	0.73	1.14	3.88	1.74	1.28	1.63	0.85	1.30	1.17
As	4.8	5.6	3.8	7.0	2.9	4.0	2.7	2.1	2.9	6.5	7.3	4.7
Se	1.97	1.98	2.37	1.53	0.94	2.06	1.57	1.85	1.58	7.33	9.05	2.94
Rb	100	101	101	72	133	143	122	93	94	57	81	76
Sr	34	28	25	62	21	43	31	28	37	33	15	19
Y	47	38	35	50	46	32	31	29	35	72	244	112
Zr	168	170	201	161	185	174	214	224	160	109	65	112
Nb	13.3	15.0	12.9	11.7	13.5	11.6	13.9	13.9	12.6	12.1	5.8	12.7
Mo	2.25	4.19	3.01	2.73	3.83	3.26	2.69	3.13	3.09	13.07	5.31	4.63
Ag	0.22	0.17	0.29	0.32	0.07	0.45	0.35	0.15	0.37	0.45	0.34	0.28
Sn	3.91	4.13	3.92	2.87	6.57	3.13	4.00	4.34	3.92	4.35	2.13	4.59
Sb	0.96	0.53	1.66	0.73	0.76	5.32	1.50	0.70	3.40	0.83	0.53	0.58
Te	19.20	3.06	4.79	5.04	1.03	8.41	5.94	2.03	4.81	13.28	25.15	28.14
Ba	300	361	362	201	503	337	547	301	348	208	160	294
La	38.9	36.5	43.1	28.5	40.5	32.4	47.5	51.7	47.7	178.1	43.8	57.7
Ce	78.2	76.7	94.6	65.3	81.8	69.3	97.1	102.3	94.3	309.7	92.6	112.3
Pr	9.6	9.2	11.1	8.1	10.0	8.3	11.1	11.8	11.0	38.6	11.6	13.3
Nd	38.6	36.6	41.7	33.1	40.0	31.8	41.3	44.1	41.6	146.0	50.9	54.1

Table 1. *Cont.*

	#1	#2	#3	#4	#5	#6	#7	#8	#9	#10	#11	#12
Sm	8.76	8.16	8.96	8.36	8.86	6.60	7.98	8.59	9.39	32.26	18.39	13.72
Eu	2.63	2.28	2.34	2.47	2.55	1.56	1.71	1.95	2.48	9.10	8.38	4.77
Gd	9.96	8.61	8.47	10.10	9.69	6.33	7.10	7.71	8.54	27.95	37.66	19.57
Tb	1.62	1.38	1.33	1.77	1.55	0.99	1.05	1.14	1.28	3.74	8.32	3.72
Dy	10.09	8.45	7.99	11.80	9.54	5.94	6.20	6.58	7.38	19.69	57.51	24.91
Ho	1.98	1.68	1.52	2.39	1.86	1.19	1.21	1.26	1.40	3.45	11.73	4.97
Er	5.50	4.64	4.24	6.50	5.35	3.40	3.44	3.48	3.83	8.92	30.50	13.29
Tm	0.78	0.65	0.59	0.90	0.79	0.49	0.49	0.50	0.53	1.22	4.13	1.87
Yb	4.87	3.98	3.76	5.50	4.97	3.11	3.14	3.12	3.26	7.42	23.81	11.04
Lu	0.69	0.59	0.54	0.77	0.74	0.46	0.48	0.48	0.48	0.93	2.83	1.40
Hf	4.57	4.48	5.43	4.46	5.14	4.72	5.79	5.94	4.29	2.83	1.81	3.02
Ta	0.85	0.86	0.97	0.70	0.97	0.95	1.10	1.08	0.90	0.82	0.33	0.70
W	135	169	211	25	172	25	92	147	70	227	715	615
Au g/t	1.03	0.37	0.19	0.23	0.12	0.03	0.16	0.25	0.22	3.46	6.14	3.28
Tl	0.69	0.24	2.45	0.24	0.31	9.78	2.59	0.77	5.10	1.31	0.18	0.20
Pb	2.27	2.28	2.40	3.03	1.23	2.11	2.12	1.87	2.23	5.34	4.52	3.21
Bi	11.71	1.60	1.11	1.23	0.32	2.66	1.34	0.72	2.01	11.55	21.88	24.08
Th	6.79	6.33	12.35	5.37	7.78	17.26	15.99	14.99	11.68	5.99	4.72	5.24
U	4.46	3.94	4.74	2.12	5.90	8.31	6.07	5.81	6.42	10.37	7.06	5.17
S wt.%	0.15	0.37	0.22	0.29	N.D.	0.06	0.13	0.24	0.22	1.35	1.01	0.47
Y/Ho	23.88	22.91	22.82	20.78	24.96	26.69	25.30	22.75	24.98	20.89	20.79	22.50
Zr/Hf	36.84	38.08	36.98	36.08	35.92	36.93	36.90	37.79	37.20	38.59	35.83	37.06
Nb/Ta	15.69	17.38	13.30	16.79	13.93	12.22	12.57	12.93	13.99	14.63	17.44	18.18
Nb/Y	0.28	0.39	0.37	0.24	0.29	0.37	0.45	0.49	0.36	0.17	0.02	0.11
La/Yb	7.99	9.17	11.45	5.18	8.15	10.41	15.11	16.56	14.63	24.00	1.84	5.22
Molar Cu/Au	159	786	1198	5571	784	4051	680	357	475	77	19	21

#1, alterd pyroxenite; #2, microgabbro; #3, gabbro; #4, ferrogabbro; #5, glimmerite; #6, quartz monzonite; #7, andesite; #8, andesitic tuff; #9, carbothermal veins; #10, carbothermal sheet; #11, highway breccia; #12, quartz breccia. N.D., not determined.

More than 17,915 rock chip, RC and diamond drill core samples from the Duck Creek area were also reviewed. Data reported in Table 2 are average analyses of 1801 individual analyses from historic mines in the Duck Creek area. This data was obtained with support from the Queensland Department of Mines, through a Cooperative Exploration Initiative (CEI) grant to Transition Resources. Data from the Mount Cobalt deposit are from Philpott [71] and Collerson [42]. Analyses of 1 m composite samples from an 896 m long diamond core drilled by Chinalco at the Elaine Dorothy deposit near Mary Kathleen (MKED0036) from Collerson [46].

Table 2. Major element analyses and trace element data for lithologies from the Duck Creek Area, with comparative data from Mount Cobalt and Mary Kathleen.

	Columbiad	Comet	Dulce	Easter Gift	Eva	Forget-Me-Not	Hideaway	Horseshoe
Number of Analyses	n = 130	n = 44	n = 61	n = 4	n = 13	n = 157	n = 66	n = 481
SiO_2	62.96	64.16	59.16	69.09	63.87	62.90	63.20	62.27
TiO_2	0.90	1.48	0.74	0.68	0.43	0.64	1.24	0.93
Al_2O_3	10.33	10.30	12.55	10.94	6.96	10.84	9.42	10.56
Fe_2O_3	16.39	15.58	15.60	11.51	20.51	15.05	18.65	15.34
MnO	0.09	0.32	0.13	0.09	0.11	0.08	0.12	0.12
MgO	4.76	2.30	5.83	3.78	3.43	6.11	2.32	5.45
CaO	1.46	3.28	2.86	0.43	3.31	1.49	2.75	2.60
Na_2O	2.14	1.28	2.03	2.52	0.74	1.74	1.07	1.83
K_2O	0.79	1.16	1.00	0.84	0.57	1.05	1.13	0.78
P_2O_5	0.18	0.14	0.10	0.12	0.08	0.11	0.11	0.13
SUM	100	100	100	100	100	100	100	100

Table 2. *Cont.*

	Columbiad	Comet	Dulce	Easter Gift	Eva	Forget-Me-Not	Hideaway	Horseshoe
Fe/(Fe + Mg)	0.63	0.77	0.57	0.61	0.75	0.55	0.80	0.59
$Na_2O + K_2O$	2.93	2.44	3.03	3.36	1.30	2.79	2.20	2.61
Trace Elements ppm								
Li	10.8	10.6	17.6	13.1	10.1	21.0	10.1	16.3
Be	1.65	1.26	0.94	0.85	0.66	1.10	1.00	1.05
Sc	21	30	25	19	18	24	24	26
V	224	329	216	213	274	215	352	244
Cr	52	54	92	43	70	81	68	55
Co	208	97	159	100	204	114	59	164
Ni	64	46	93	45	108	85	102	67
Cu	704	2544	5789	11,596	19,414	4645	1727	6382
Cu wt.%	0.07	0.25	0.58	1.16	1.94	0.46	0.17	0.64
Zn	28	27	37	22	29	36	41	34
Ga	20	15	22	14	14	21	15	19
Rb	37	50	47	31	26	74	54	30
Sr	30	58	50	16	24	36	60	40
Y	23	29	19	36	14	15	23	20
Zr	103	120	103	126	35	68	102	85
Nb	7.0	8.2	6.5	4.4	1.8	4.4	8.1	5.5
Mo	1.99	0.64	2.96	0.45	1.38	1.56	1.11	2.89
Pd	2.92	3.24	7.05	2.83	20.93	6.42	7.42	8.89
Ag	0.15	0.34	0.35	0.33	0.98	0.44	0.90	0.40
Sn	1.81	1.84	1.43	1.80	2.46	1.71	1.71	1.74
Sb	26.3	0.63	0.37	0.40	0.50	0.43	2.39	0.38
Cs	1.45	1.52	1.46	0.79	1.05	2.76	1.28	1.23
Ba	176	283	239	118	179	217	191	177
La	19.5	20.2	19.9	13.2	6.2	10.7	16.6	14.2
Ce	39.2	46.2	41.7	27.3	13.0	22.1	36.0	30.1
Pr	4.6	5.2	5.0	3.6	1.8	2.7	4.3	3.7
Nd	18.3	21.5	19.6	15.6	7.7	11.1	17.4	15.3
Sm	4.02	5.00	4.05	4.41	1.95	2.56	4.08	3.50
Eu	1.03	1.46	0.90	1.15	0.48	0.62	1.08	0.83
Gd	4.26	5.55	3.82	5.50	2.20	2.71	4.31	3.65
Tb	0.70	0.85	0.57	0.91	0.36	0.44	0.68	0.59
Dy	4.30	5.43	3.62	6.11	2.40	2.90	4.33	3.82
Ho	0.87	1.11	0.72	1.27	0.51	0.60	0.88	0.78
Er	2.55	3.57	2.13	4.15	1.64	1.78	2.66	2.29
Tm	0.36	0.52	0.31	0.63	0.24	0.27	0.38	0.34
Yb	2.30	3.47	2.04	4.25	1.59	1.65	2.45	2.09
Lu	0.34	0.56	0.31	0.66	0.25	0.25	0.37	0.33
Hf	3.03	3.18	2.83	3.42	0.95	1.98	2.77	2.55
Ta	0.53	0.60	0.48	0.34	0.12	0.32	0.59	0.42
W	3.31	12.78	1.91	4.38	5.30	3.52	1.69	3.83
Pt	3.66	3.44	6.14	1.40	12.68	6.46	3.94	7.41
Au ppm	0.02	0.12	0.04	0.04	2.36	0.07	0.07	0.06
Tl	0.16	0.20	0.20	0.10	0.12	0.29	0.24	0.13
Pb	4.12	4.24	2.16	19.33	8.24	1.85	40.20	2.02
Bi	0.85	1.00	1.19	0.41	3.85	1.33	4.19	0.68
Th	5.49	6.14	6.66	5.89	1.10	3.39	5.53	3.62
U	2.27	1.97	2.13	4.56	3.44	2.37	1.55	1.99
TREE ppm	102	121	105	89	40	60	96	81
logAg/Au	0.91	0.46	0.98	0.90	−0.38	0.78	1.12	0.82
Molar Cu/Au	122,967	66,077	495,563	866,068	25,471	195,163	78,261	326,323
Y/Ho	26.29	26.48	26.65	28.42	27.87	25.52	26.09	25.35
Zr/Hf	33.90	37.63	36.46	36.87	36.44	34.48	36.73	33.53
Nb/Ta	13.41	13.84	13.50	13.02	14.52	13.84	13.62	13.12
Nb/Y	0.31	0.28	0.34	0.12	0.13	0.29	0.35	0.28
Nb + Y	29.95	37.70	25.59	40.46	16.09	19.84	31.12	25.26

	Junction	Micawber	Mountain Maid	New Dollar	Ready Rhino	Success	Mount Cobalt	Elaine Dorothy, Mary Kathleen
Number of Analyses	n = 52	n = 67	n = 216	n = 168	n = 145	n = 196	n = 3	n = 640
SIO_2	55.62	60.80	64.04	61.79	61.31	65.01	46.33	46.74
TiO_2	0.94	0.64	1.06	0.86	0.86	1.18	1.51	4.78
Al_2O_3	14.01	12.44	9.94	10.80	11.61	10.08	13.45	0.18
Fe_2O_3	15.37	13.91	15.53	15.70	14.38	16.98	17.74	19.02
MnO	0.13	0.11	0.10	0.11	0.11	0.16	0.16	0.32

Table 2. *Cont.*

	Junction	Micawber	Mountain Maid	New Dollar	Ready Rhino	Success	Mount Cobalt	Elaine Dorothy, Mary Kathleen
MgO	6.50	5.66	4.28	6.08	6.69	3.21	9.20	3.99
CaO	3.07	2.65	1.85	1.69	2.04	1.34	5.05	23.65
Na_2O	3.00	2.30	1.71	1.43	1.53	0.98	1.88	0.65
K_2O	1.20	1.38	1.29	1.43	1.33	0.93	4.55	0.26
P_2O_5	0.17	0.11	0.20	0.12	0.15	0.11	0.12	0.42
SUM	100	100	100	100	100	100	100	100
Fe/(Fe + Mg)	0.54	0.55	0.65	0.57	0.52	0.73	0.49	0.85
$Na_2O + K_2O$	4.21	3.68	3.00	2.86	2.86	1.92	4.68	0.90
Li	19.7	17.2	14.3	25.9	29.1	15.7	26.7	6.89
Be	1.48	1.10	1.63	1.18	1.25	1.31		1.71
Sc	32	26	23	29	31	27	52	3.34
V	250	201	246	263	265	329	573	79.71
Cr	75	63	54	74	66	66	113	9.18
Co	60	124	156	80	76	208	148	104
Ni	67	101	62	70	80	67	147	203
Cu	187	2197	2932	4796	2774	4820	184	2039
Cu wt.%	0.02	0.22	0.29	0.48	0.28	0.48	0.02	0.20
Zn	42	38	33	32	38	25	34	23.44
Ga	22	21	19	19	19	17	36	15.45
Rb	55	79	73	65	61	43	423	11.16
Sr	69	51	39	29	48	33	59	18.90
Y	25	18	25	18	22	23	32	38.78
Zr	125	97	117	75	85	118	84	46.29
Nb	8.2	6.0	8.1	4.4	5.2	7.2	7.7	9.70
Mo	1.51	1.45	2.07	1.29	1.33	0.92	1.50	1.83
Pd	9.13	7.24	2.79	7.07	8.22	4.44	1.80	
Ag	0.18	0.16	0.32	0.29	0.28	0.42	1.67	0.11
Sn	2.12	1.40	1.82	1.33	1.43	2.39	0.08	45.72
Sb	0.57	0.33	0.33	0.40	0.48	0.53	0.43	0.33
Cs	2.89	4.06	2.66	3.39	2.68	1.18	13.78	0.36
Ba	293	292	217	189	234	200	461	52.6
La	34.1	17.5	20.4	13.6	14.2	22.9	152.6	159.5
Ce	66.6	36.4	43.1	27.4	29.4	46.0	270.4	303.3
Pr	7.7	4.4	5.2	3.3	3.7	5.5	30.9	29.5
Nd	29.7	17.4	20.8	13.7	15.4	21.9	119.4	101.24
Sm	5.85	3.71	4.58	3.18	3.67	4.83	25.89	16.39
Eu	1.63	0.82	1.16	0.82	0.94	1.35	2.65	3.49
Gd	5.38	3.68	4.80	3.44	3.97	4.78	19.38	11.69
Tb	0.79	0.55	0.79	0.55	0.63	0.73	2.22	1.48
Dy	4.83	3.47	4.79	3.50	4.07	4.51	9.58	7.28
Ho	0.95	0.68	0.97	0.71	0.82	0.89	1.44	1.28
Er	2.75	2.04	2.84	2.10	2.43	2.62	3.35	3.22
Tm	0.40	0.29	0.41	0.30	0.34	0.37	0.43	0.43
Yb	2.54	1.95	2.63	1.93	2.24	2.46	2.39	2.59
Lu	0.38	0.31	0.39	0.29	0.34	0.37	0.31	0.39
Hf	3.47	2.68	3.25	2.13	2.37	3.20	2.30	1.09
Ta	0.61	0.45	0.58	0.31	0.36	0.54	0.23	0.26
W	3.34	2.04	3.27	3.58	4.26	3.10	1.00	13.76
Pt	8.43	5.52	2.76	6.66	7.52	3.97	1.50	
Au ppm	0.00	0.03	0.03	0.03	0.02	0.15	0.01	0.04
Tl	0.23	0.28	0.25	0.19	0.23	0.18	0.92	0.05
Pb	1.92	1.96	2.19	2.42	2.13	4.26		9.80
Bi	0.25	0.58	3.94	1.26	0.93	2.16	0.06	2.81
Th	8.03	6.52	5.79	2.37	3.75	6.02	1.22	55.81
U	2.43	2.23	2.57	2.06	1.93	2.17	0.86	17.95
TREE ppm	164	93	113	75	82	119	641	642
logAg/Au	1.62	0.74	1.06	0.94	1.06	0.45	2.44	0.41
Molar Cu/Au	133,087	230,183	333,822	438,564	345,827	99,015	94,882	143,049
Y/Ho	26.19	26.69	26.36	25.83	26.45	25.89	22.03	30.39
Zr/Hf	36.14	36.17	36.06	35.38	36.09	36.87	36.52	42.38
Nb/Ta	13.30	13.52	14.01	14.08	14.38	13.38	32.86	37.20
Nb/Y	0.33	0.33	0.32	0.24	0.24	0.31	0.24	0.25
Nb + Y	33.09	24.30	33.57	22.69	26.90	30.21	39.47	48.48

No generative artificial intelligence (GenAI) assistance was used in the preparation of this manuscript.

5. Results

Figure 11 shows the areal extent and Cu, Au, Pd, Pt, Ni, Co and Sc anomalism in different deposits listed in Table 2 from the Highway–Duck Creek area. As this elemental anomalism extends for a strike length of more than 18.4 km, it is clear that a very large mineral system lies west and at depth below the Highway epithermal domain.

The region is currently under active resource definition by Transition Resources. The Highway epithermal mineralisation exhibits significant concentrations of precious and critical metals (Table 1), e.g., Au intersections of up to 11 m @ 9.58 g/t, 7 m @ 9.02 g/t Au and 2 m @ 41.2 g/t Au. The system is also rare earth element-rich with up to 157 ppm Dy_2O_3 and 23 ppm Tb_4O_7. Other key critical elements in the Highway system include WO_3 and Sc_2O_3, which range up to 1793 ppm and 64 ppm, respectively.

The current global gold resource for the extreme northern segment of the Highway epithermal corridor at a depth of 125 m is 1.2 Mt @ 3.1 g/t Au and 1600 ppm WO_3, plus significant HREEs, Co and Sc. Although limited resource drilling has been undertaken in the Duck Creek porphyry system, assays from a small segment of the exploration target indicate an inferred JORC resource of 5.44 Mt @ 1.45 wt.% Cu, 0.11 g/t Au and 158 ppm Co. The current global resource for Duck Creek porphyry is estimated to contain 6.5 Mt @ 1.57 wt.% Cu, 0.12 g/t Au.

5.1. Metallogenic Affinity

5.1.1. K_2O-SiO_2 and Th-Co Discrimination Plots

CEI data for the Duck Creek deposits and the mean compositions of the Highway lithologies are plotted in the K_2O and SiO_2 discrimination projection of Peccerillo and Taylor [72] to understand the petrological affinity of the igneous source responsible for the formation of the Highway–Duck Creek mineral system. The Duck Creek data show a broad range of compositions extending from shoshonite to low K calc-alkaline (Figure 12a).

The mean data for the different Highway lithology assemblages in Figure 12b is more coherent and falls within the field from high K to medium K. The spectrum of variation shown by K_2O is interpreted to largely be caused by the loss of K_2O during the phyllic and propylitic alteration event that permeated the system following the crystallisation of the primary igneous lithologies [74]. In addition, as these lithologies show phyllic or propylitic alteration, it is likely that all have either lost or gained Si.

To circumvent the effect of loss or gain of K during post-crystallisation alteration, Hastie et al. [73] suggested using Th as a proxy for K and Co as a proxy for Si and proposed a discrimination projection that was more robust to alteration. Figure 12c–f shows Th and Co data for Highway and Duck Creek lithologies. They indicate that the dominant metal source at Highway and Duck Creek was an alkaline (high K) igneous suite, although samples from some Duck Creek deposits, e.g., Ready Rhino, New Dollar, Mountain Maid and Horseshoe, exhibit a secondary calc-alkaline to tholeiitic petrologic vector.

These divergent trends are interpreted to indicate the presence of two petrological/mineralising systems in the Duck Creek area. First, a subduction-related porphyry mineralising event with a magmatic arc source, which formed during subduction and back arc extension. This was followed by a second metallogenic event, after collision and closure of an ocean basin east of the North Australian Craton. It is likely that a palaeo-slab tear was accreted to the North Australian Craton lithosphere at this time, thereby providing a window that facilitated the ingress of plume magmas into the mantle wedge and subcontinental lithosphere. The post-tectonic tholeiitic to alkaline suite thus provided the metal source for the formation of a later porphyry system with high-level epithermal carapace. In this regard, the identification of a potassic magmatic source has significant implications for the metal endowment because some of the largest porphyry systems are hosted by K-rich

magmas [75]. As continental collision zone porphyry deposits are typically hosted by potassic and ultrapotassic magmas [7,54,76], evidence for the presence of such a magmatic source for the Highway Duck Creek system provides additional support for the continental collision zone porphyry model.

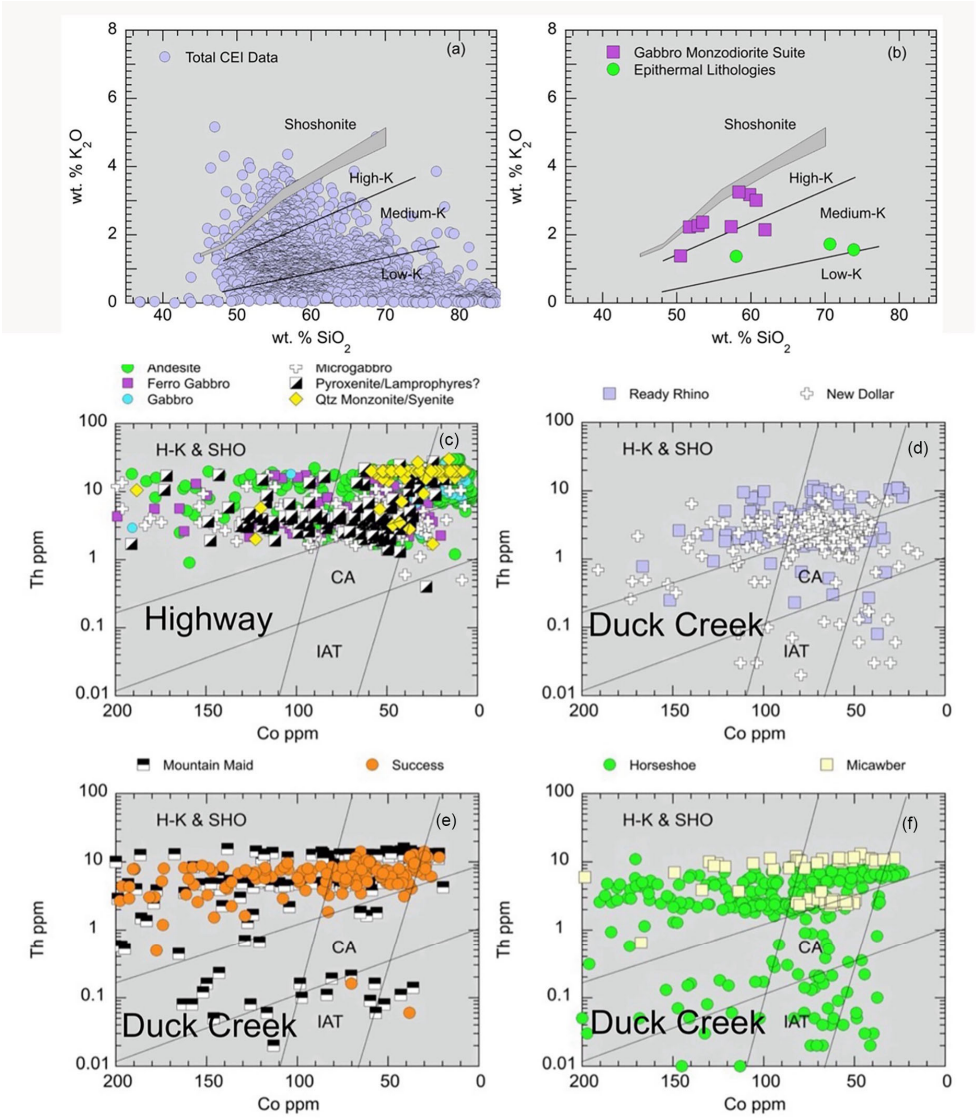


Figure 12. K_2O vs. SiO_2 discrimination plot for calc-alkaline, high potassium and shoshonite igneous suites after Peccerillo and Taylor [72] showing (**a**) data for Duck Creek deposits (CEI data set), and (**b**) average compositions of gabbro-monzodiorite suite lithologies and epithermal lithologies from the Highway epithermal system (Table 1). (**c**–**f**) shows data from Highway and Duck Creek plotted in Th vs Co space showing the fields of shoshonite and high K calc alkaline, calc alkaline and Island arc tholeiites after [73].

The identification of a potassic magmatic source for the Highway–Duck Creek mineral system also has important regional implications. For example, this potassic signature is also seen at Mount Cobalt (Figure 13a,b) and at the Elaine Dorothy deposit near Mary Kathleen (Figure 13c,d). This signature is also prominent in many of the "IOCG" deposits in the Cloncurry area (Figure 13e).

5.1.2. Multi-Element Geochemical Variation

Primitive mantle-normalised multi-element plots, where elements are arranged in order of increasing compatibility, are an effective way to compare geochemical data for

different protoliths. The primitive mantle values used for element normalisation are either from McDonough and Sun [77] or Lyubetskaya and Korenaga [78]. Analyses of the Duck Creek deposits and the different Highway lithologies are compared in Figure 14a,b. The two systems exhibit broadly uniform shaped patterns, with positive spikes in W, U, Pb, P and Li and negative spikes in Ba, Th, Nb, Ta and Sr. The pronounced depletion in Sr is a common feature seen at both Duck Creek and Highway. It could reflect the fact that early fractionation of a Ca-Sr component (possibly a carbonatite) has occurred during the evolution of the source magma. Alternatively, the widespread Sr depletion seen at Highway and Duck Creek could be alteration induced [79–81]. Highway also shows a pronounced negative Ti spike, which is absent at Duck Creek and suggests the fractionation of a Ti-bearing mineral into the gabbro–monzogabbro intrusion that underlies the Mitakoodi anticline.

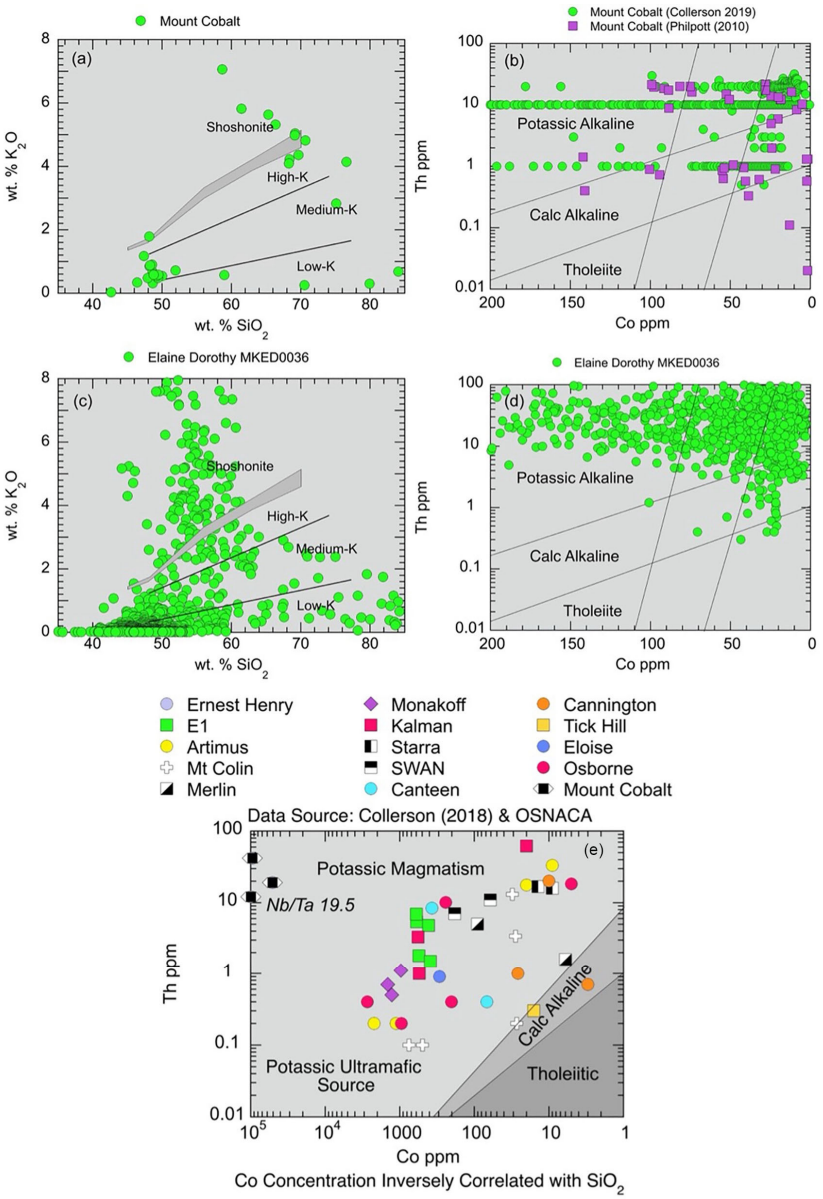


Figure 13. K_2O vs. SiO_2 and Th vs. Co plots comparing data for selected mineral deposits in the eastern NWMP. (**a**,**b**) Mount Cobalt, (**c**,**d**) Mary Kathleen–Elaine Dorothy and (**e**) deposits classified as "IOCG" systems in the eastern NWMP and southern NWMP. The majority of "IOCG" deposits plot within the potassic field, using Th vs. Co systematics that extend from ultramafic Mt Cobalt to felsic compositions. Mount Cobalt has a plume-like Nb/Ta ratio of 19.5. Data sources [42,45,71,82].

In addition to the significant level of W enrichment seen in all Highway lithologies, they are also significantly enriched (50 to 100× PM levels) in the rare earth elements (REEs). These include the high-value heavy rare earth elements, Dysprosium (Dy) and Terbium (Tb), which are hosted by xenotime and monazite. For example, average compositions are 8.32 ppm Tb and 57.51 ppm Dy breccia (n = 15), 3.74 ppm Tb and 19.69 ppm Dy carbothermal (n = 435) l and 3.72 ppm Tb and 24.91 ppm Dy epithermal quartz breccia (n = 163). These lithologies are also significantly enriched in Au, averaging 6.14 g/t (breccia), 3.46 g/t (carbothermal sheets) and 3.28 g/t (quartz breccia).

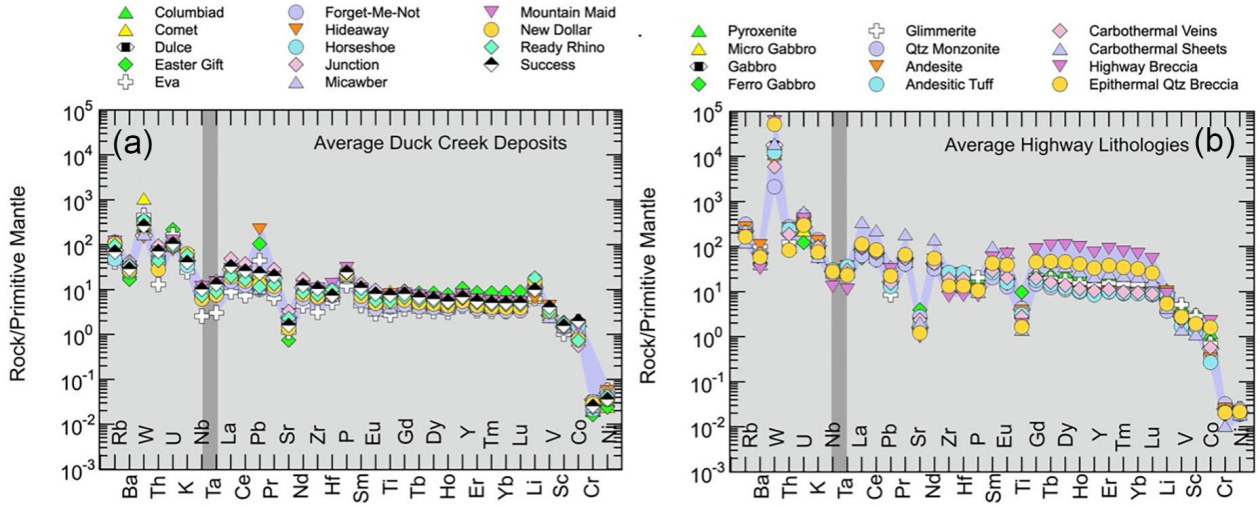


Figure 14. Primitive mantle-normalised multi-element variation diagrams showing (**a**) average compositions for a selection of Duck Creek deposits and (**b**) average compositions of Highway lithologies. The patterns are remarkably similar, which supports the interpretation that they are genetically related systems. Furthermore, lithologies from both systems show distinctive negative spikes in Sr. This is interpreted to have been caused by Sr loss from the entire mineral system during pervasive hydrothermal alteration.

Although the level of W enrichment in all Highway lithologies is significantly greater than at Duck Creek, the overall similarity in pattern, with relatively consistent immobile-incompatible element ratios, results in parallel profiles at Duck Creek and Highway. This supports the model that they are related systems and that the metals in the Highway epithermal system were delivered by fluids derived from the deeper Duck Creek system.

To discriminate between different mineral deposit styles, with specific reference to the IOCG class of deposit, Brauhart and Groves [34] proposed the use of multielement plots normalised to average crustal abundance [83]. This projection highlights the granitophile La and U enrichments seen in both IOCG and some porphyry systems (Figure 15).

The projection also highlights the enrichment in an 'ultramafic' suite of elements, such as the transition elements (Co-Ni) and the platinum group metals (Pd-Pt). In these plots, the presence of spikes in these elements in a mineral system geochemical profile indicates the role of a mantle continental collision zone porphyry system rather than a crustal component in the metallogenic process.

The principal focus of the Brauhart and Groves [34] publication was to compare the chemical variability of Australian intracratonic deposits, classified as IOCG and ISCG systems. However, in some locations, e.g., Chile [32] and the Gawler [31], Cu-Au porphyry deposits occur close to IOCG systems. Cu-Au porphyry deposits also occur in cratonic settings [7], especially in collisional cratonic environments, like the eastern margin of the North Australian Craton [52]. Thus, to provide a more representative platform for comparing between IOCG and Cu-Au porphyry systems, crustal abundance multi-element

normalised plots for representative Cu-Au porphyry deposits using data from the OSNACA database [83] are shown in Figure 15. Porphyry systems exhibit a downward trend from Fe to Ni, but they also show positive spikes in Pd, Cu, Au, Te and W.

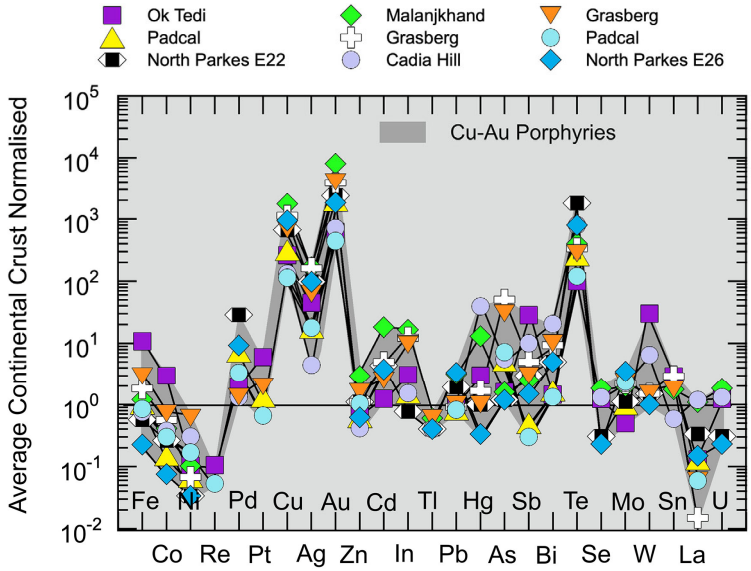


Figure 15. Ore and pathfinder element plots showing data for Cu-Au porphyries from the OSNACA database [82] normalised to average crustal abundances from Rudnick and Gao [83].

Crust-normalised data for the Highway mineral system lithologies are shown in Figure 16a,b. The Highway patterns are remarkably similar to the Cu-Au porphyry field with prominent spikes in Au, Te and W. It is also enriched in Co, La and U, relative to Cu-Au porphyries that are hosted by K-rich igneous lithologies. The depletion at Highway reflects the fact that Cu has largely been sequestered by sulphide precipitation into the underlying Duck Creek porphyry system. Such depletion in Cu is a typical feature of epithermal mineralisation above porphyry systems [84].

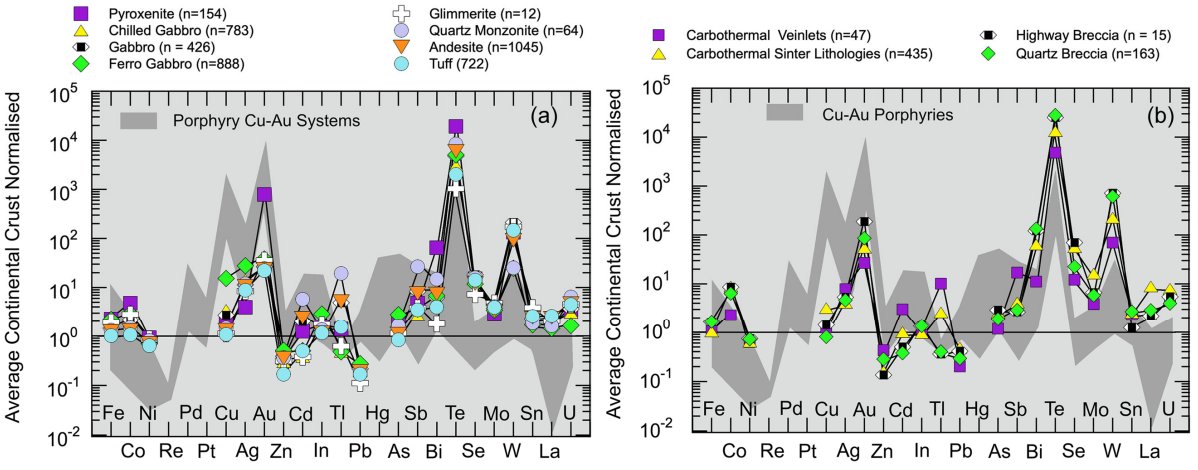


Figure 16. Ore and pathfinder element plots normalised to average crustal abundance, showing data for average Highway lithologies (n = number of analyses). (**a**) shows data for Highway mafic and calc alkaline lithologies and (**b**) shows data for epithermal carbothermal rocks and breccias. The patterns are remarkably similar to the Cu-Au porphyry field, except that the Highway epithermal field is Cu depleted because Cu has largely been sequestered into the underlying Duck Creek porphyry system. Such depletion in Cu is a typical feature of epithermal mineralisation above the porphyry systems. The Highway system also exhibits prominent spikes in Te and W. It is also enriched in Co, La and U, relative to Cu-Au porphyries that are hosted by K-rich igneous lithologies.

Crustal abundance multi-element normalised plots for several Duck Creek deposits, i.e., Success, Mountain Maid, Horseshoe, Dulce, Eva, Furnace, Glory Hole, Comet and Daisey are shown in Figure 17.

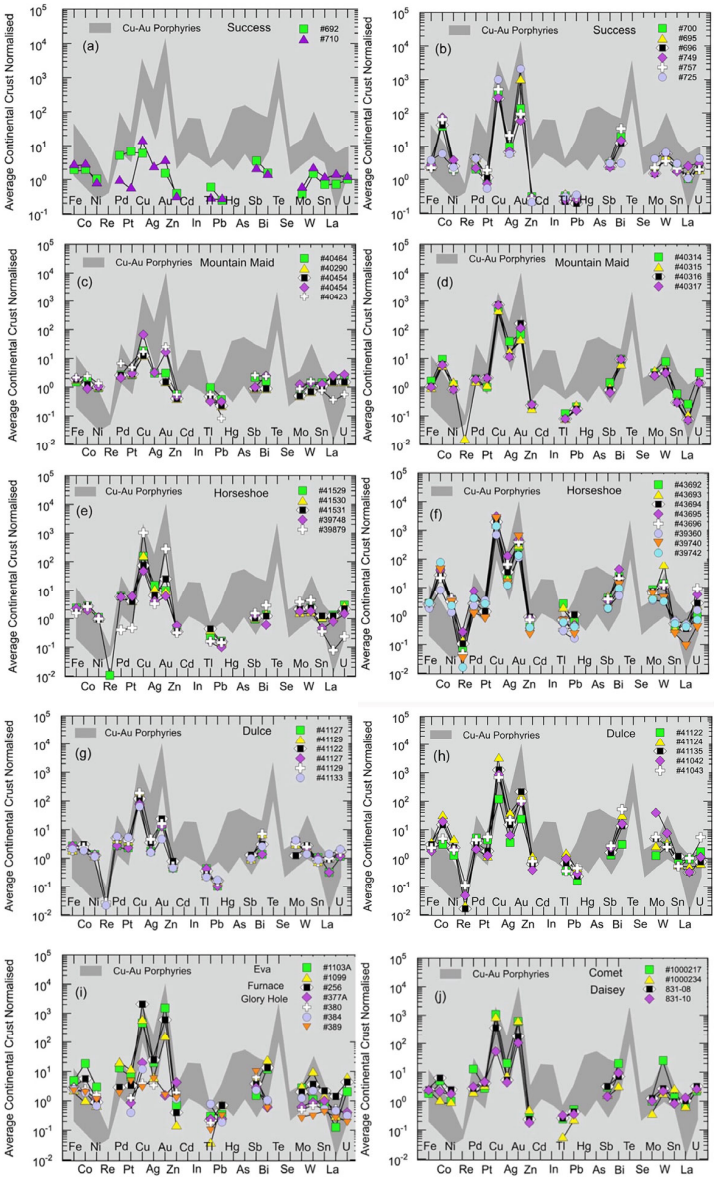


Figure 17. Ore and pathfinder element plots normalised to average crustal abundance for several of the Duck Creek deposits, Success, Mountain Maid, Horseshoe, Dulce, Eva, Furnace, Glory Hole, Comet and Daisy. Success (**a**,**b**), Mountain Maid (**c**,**d**), Horseshoe (**e**,**f**) and Dulce (**g**,**h**) have enrichment patterns similar to the Cu-Au porphyry field. A subgroup of Co-rich samples from Eva, Furnace and Glory Hole (**i**,**j**) from Comet and Daisey indicates the possible involvement of two metal sources: a subduction-generated component similar to the porphyry field and an ultramafic to mafic component most likely derived from the post-tectonic tholeiitic to alkalic plume system.

Samples exhibit topologies that either resemble porphyries with a downward trend from Fe to Ni and the positive spikes in Cu, Au, Te and W, or they resemble the Highway sub-pattern with positive spikes in Co, as well as in Cu, Au, Te and W. For example, samples from Success (Figure 17a,b), Mountain Maid (Figure 17c,d), Horseshoe (Figure 17e,f), Dulce (Figure 17g,h), as well as at Eva, Furnace, Glory Hole, Comet and Daisy (Figure 17i,j). The presence of these different patterns suggests the possible involvement of two metal sources in the metallogenic evolution of the Duck Creek system, viz., a subduction-generated com-

ponent, generating patterns like the porphyry field, and an ultramafic to mafic component most likely associated with the post-tectonic tholeiitic to alkalic plume component.

5.1.3. Metal Source Constraints from Te, Cu, Ni Systematics

Post-subduction geodynamic settings are characterised by significant mantle-to-crust fluxes of metals and volatiles. Te is a tracer of this flux and of the magmatic and hydrothermal processes that drive the flux. Post-subduction magmato-hydrothermal systems are Te-enriched and exhibit both incompatible and chalcophile behaviour. At magmatic temperatures (>1000 °C), Te has chalcophile behaviour like Au, Cu and the PGEs. Thus, at magmatic temperatures, Te enters sulphide melts, which fractionate and form Pt–Pd–telluride melts at ~900 °C and then Pt–Pd–telluride minerals at <400 °C [85,86]. However, under hydrothermal conditions, at ~300 °C, Te is mobilised as chloride complexes [87], as polytellurides in S- and CO_2-rich fluids [88] and as telluride–bismuthide melts [88]. Thus, Te is an ideal tracer of both magmatic and hydrothermal processes, providing important information regarding mantle-to-crust fluxes of metals showing spatial and genetic links between deep magmatic Ni–Cu–PGE–Au–Te mineral systems and shallower, alkali-enriched porphyry–epithermal Cu–Au-(PGE-Te) deposits [89].

As a result of this behaviour, Holwell et al. [84] demonstrated that Ni, Cu and Te systematics are effective vectors to resolve petrogenetic processes and metallogenic sources. Figures 18 and 19 show Cu, Ni and Te systematics for representative samples from Highway and from several Duck Creek deposits. These figures also show compositional fields of porphyry, epithermal, carbonatite, magmatic Cu-Ni-PGE and IOCG mineralisation.

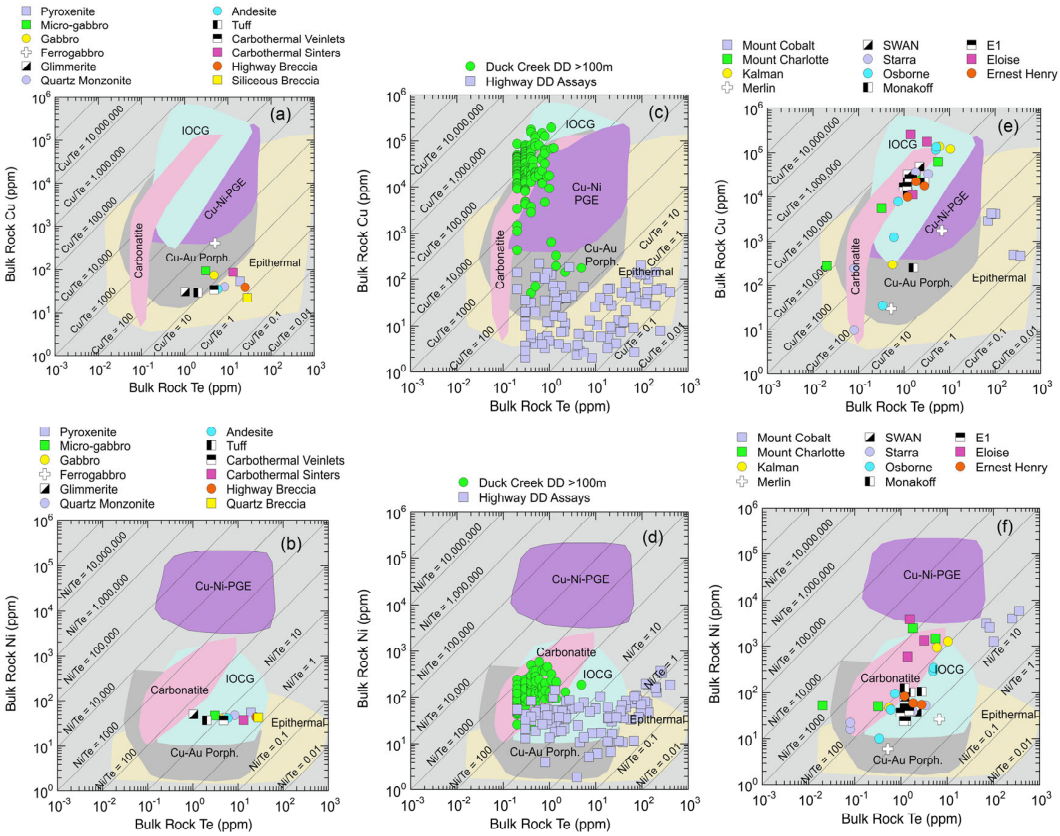


Figure 18. Cu vs. Te and Ni vs. Te covariation showing that the Highway samples fall in the epithermal field. Comparative fields are from data in [82]. The Cu-Au porphyry field has been enhanced with data for the Skouries Cu-Au porphyry [86]. (**a**,**b**) show data from Highway. (**c**,**d**) show data from Highway and Duck Creek, and (**e**,**f**) show data for Cloncurry "IOCG" deposits for comparison.

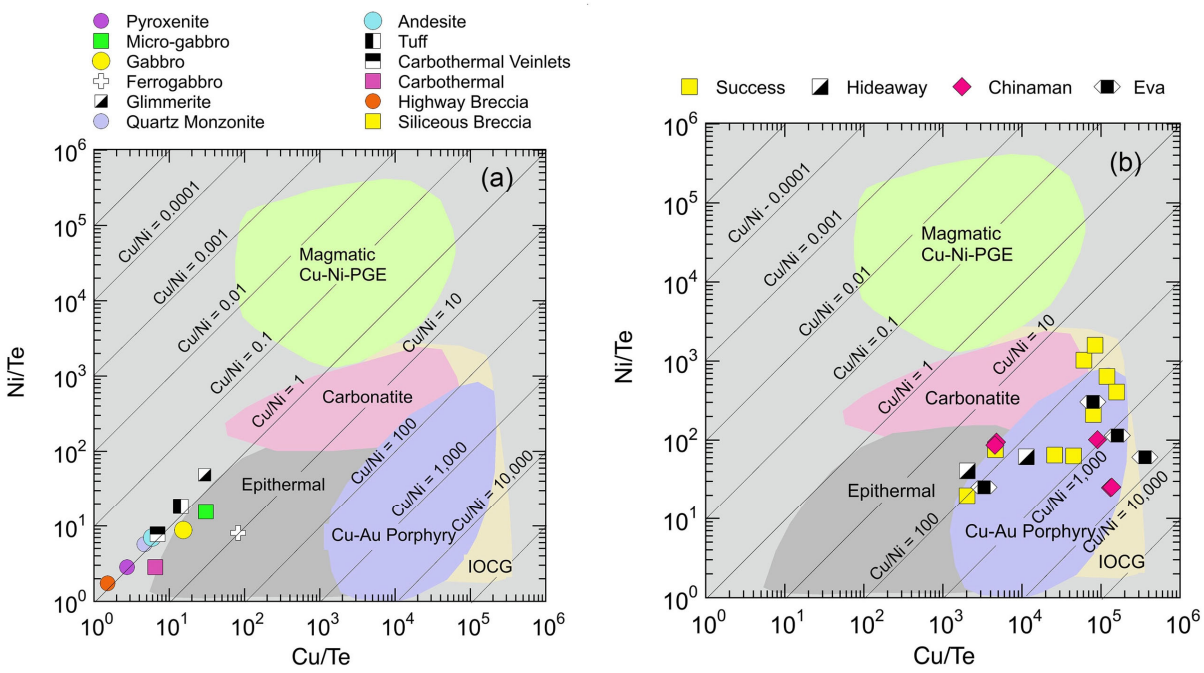


Figure 19. Plot of Ni/Te and Cu/Te, showing that the Highway samples fall in the epithermal field. Comparative fields are from Brauhart et al. [82]. The Cu-Au porphyry field has been enhanced with data for the Skouries Cu-Au porphyry [86]. (**a**) Shows data for average Highway lithologies and (**b**) shows data for samples from Duck Creek where Te analyses had been undertaken.

Figure 18a,b shows the compositional variability of individual Highway lithologies in Cu-Te and Ni-Te space. They lie within the epithermal field and in Cu-Te space within the Cu-Au porphyry field. Analyses of diamond drill hole samples from Duck Creek at a depth of >100 m (Figure 18c,d) show an even more prominent compositional difference between the volatile-dominated Highway system and sulphide-dominated Duck Creek systems. Figure 18e,f show data for NWMP deposits that are classified as IOCG systems [82].

The projection also highlights the enrichment in the 'ultramafic' suite of elements, such as the transition elements (Co-Ni) and the platinum group metals (Pd-Pt). In these plots, the presence of spikes in these elements in a mineral system geochemical profile indicates the role of a mantle-derived rather than a crustal component in the metallogenic process.

Covariation between Ni/Te and Cu/Te (Figure 19) shows a clear discrimination between epithermal and porphyry systems, with the Te-rich Highway lithologies plotting in the epithermal field along a Cu/Ni ratio vector of ~1 and Success, Hideaway, Chinaman and Eva showing the effect of Cu enrichment and plotting within the porphyry field.

5.1.4. Chalcophile Element and Highly Siderophile Element Systematics

Chalcophile element fertility or the chalcophile metal abundance and the availability of sulphur during source magma evolution, is a critical factor required to enable the formation of porphyry Cu ± Au deposits. Some mineralised porphyry systems are known to contain hydrothermal Pd and Pt [14], showing that hydrothermal fluids can mobilise Pd and Pt, and in rare cases, porphyry Cu deposits can contain up to 2400 ppb Pd (e.g., Skouries Cu porphyries, Greece; [13]). Park et al. [90] have shown that the platinum group elements (PGEs) can be used as a tracer for chalcophile element fertility during magma evolution.

Recent studies on platinum group geochemistry of subvolcanic rocks associated with porphyry Cu ± Au deposits [91–93] have suggested that the relative timing of fluid and sulfide saturation plays an important role in the formation of porphyry Cu ± Au deposits. The PGEs are used in preference to Cu and Au for two reasons. First, their partition coefficients

in immiscible sulfide melts are one to two orders of magnitude higher than those of Cu and Au, respectively [94]. Second, because they are appreciably less affected by alteration than Cu and Au, they are more likely to preserve original igneous geochemistry [95,96]. The relative abundances of Cu and Pd porphyry systems are shown in Figures 20 and 21. Figure 20 shows covariation between Cu and Pd in several major porphyry Cu and Au-Cu deposits. Although Cu varies by several orders of magnitude in Bingham Canyon and Cadia Hill, it does not correlate with increases in Pd, as might be expected if Pd were an important component in the hydrothermal fluid. This indicates that the abundance of Pd is controlled by the chemistry of the porphyry host magma.

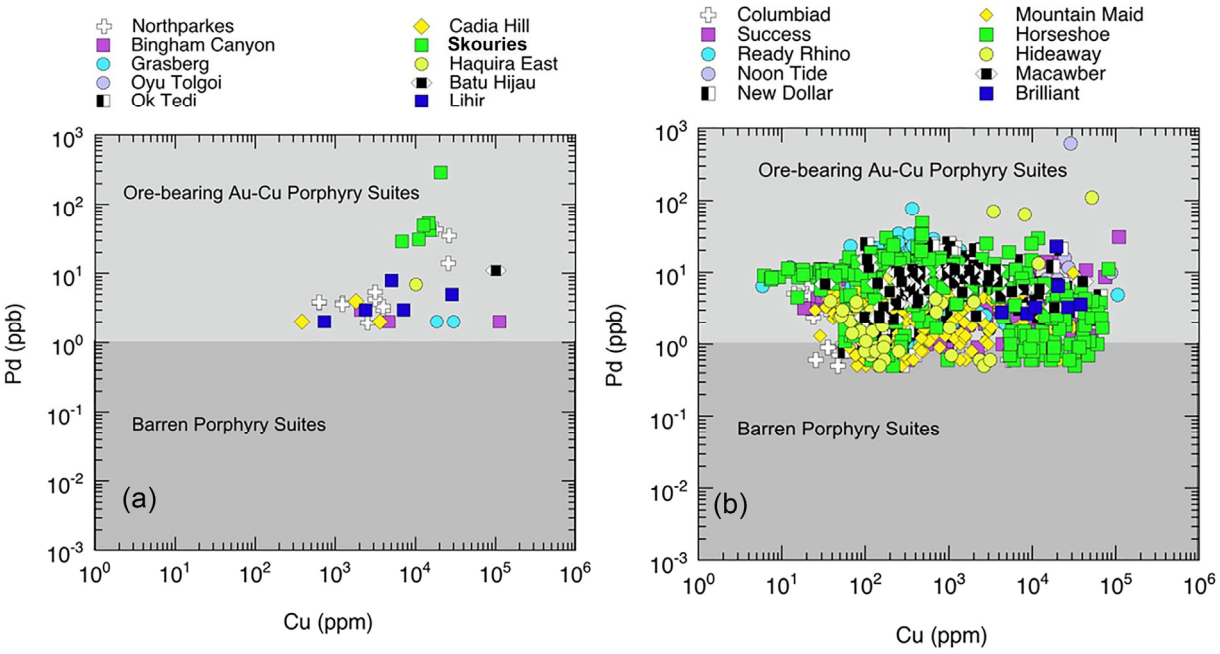


Figure 20. Covariation between Cu and Pd in (**a**) several major porphyries Cu and Au-Cu deposits and (**b**) deposits from the Duck Creek area. The similarity in Pd–Cu systematics is striking, showing that the Duck Creek system is Pd-rich with compositions that resemble the Skouries Cu-Au porphyry.

Samples from the Duck Creek system all plot with the Cu-Au porphyry field (Figure 20b). Many of these are significantly enriched in Pd; in fact, some samples from Noontide, Hideaway and Success have similar Pd contents (Figure 20b) to the PGE-rich Skouries Cu-Au (Pt, Pd, Te) porphyry (Figure 20a) [89].

This is also shown in Figure 21, which compares Pd with Cu/Pd and Pd/MgO with Pd/Pt ratios. Figure 21a,b shows that the Duck Creek Porphyry system lies on a similar sulphide segregation fractionation vector in Pd vs. Cu/Pd space to Skouries and several other gabbro-hosted porphyry systems, e.g., Beleuti, Akcha, Kalmakyr, Elasite, Assarel, Medet and Tsar Assen [97], that all occur in collisional orogenic environments. Importantly, the Highway and Duck Creek lithologies (Figure 21c) and the gabbro-hosted porphyry systems (Figure 21d) all define a trend indicating that metallogenesis involved S undersaturated fractionation.

The remarkable similarity between Cu, MgO and Pd systematics of the Duck Creek deposits with porphyry mineral systems such as Cadia, Bingham Canyon, Grasberg and Northparkes, Beleuti, Akcha, Kalmakyr, Elasite, Assarel, Medet and Tsar Assen, provides vector support for the model that the Duck Creek area is likely underlain by a significant porphyry Cu-Au mineral system. The similarity between the Duck Creek system and PGE-Cu systematics of other mafic-hosted porphyries is remarkable, confirming the validity of the mineral system interpretation.

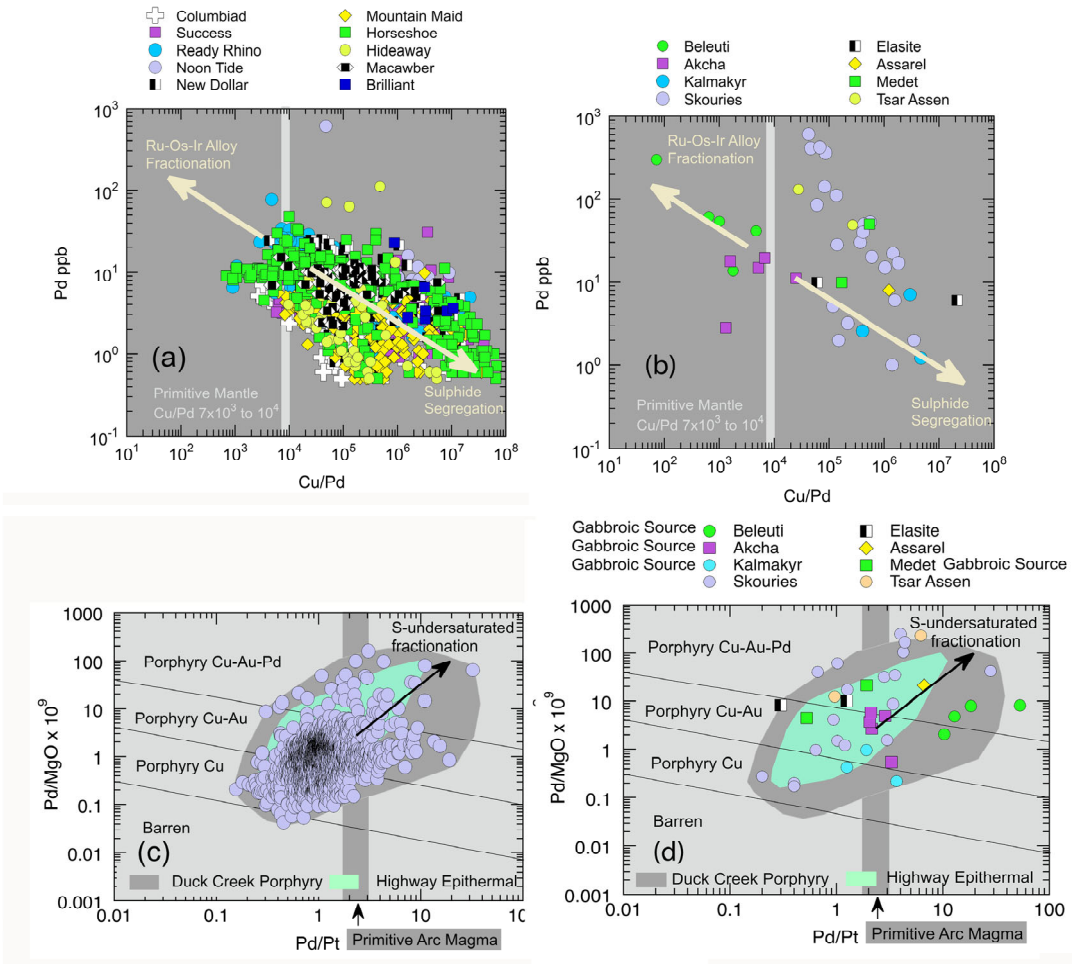


Figure 21. (**a**,**b**) Pd and Pd/Cu systematics showing that the Duck Creek Porphyry system lies on a similar sulphide segregation fractionation vector to that exhibited by Skouries and by several other gabbro-hosted porphyry systems, e.g., Beleuti, Akcha, Kalmakyr, Elasite, Assarel, Medet and Tsar Assen [97]; (**c**,**d**) Highway, Duck Creek and the gabbro-hosted porphyry systems (**d**) define similar trends, indicating metallogenesis involved S-undersaturated fractionation.

5.1.5. Deducing Redox Conditions Using Scandium and Vanadium Systematics

In low-oxygen fugacity magmas, V^{3+} behaves like Sc^{3+} and substitutes for Fe in amphibole and pyroxene. Thus, the V/Sc ratios of reduced magmas remain constant at around 7 [98]. However, in hydrous oxidised porphyry magmas, V behaves as an incompatible element and is enriched in these melts. Scandium, on the other hand, substitutes into clinopyroxene and hornblende [99]. Hence, in oxidised and hydrous melts, crystallisation of hornblende and clinopyroxene lowers Sc in the melt, causing an increase in V/Sc ratios. Although hornblende fractionation is commonly interpreted to play a role in V/Sc fractionation trends [99,100], clinopyroxene has a higher partition coefficient for Sc [100] and thus formation of clinopyroxene-rich cumulate lithologies would be expected to be Sc-rich and be characterised by low V/Sc ratios. The pyroxene-bearing lithologies at Mount Cobalt, with 52 ppm Sc and 575 ppm V and a V/Sc ratio of 11, confirm this interpretation. Thus, Sc and V systematics in the Highway–Duck Creek mineral system provide useful information regarding the redox history of the system, where fertile porphyry Cu magmas show a trend of increasing V/Sc with increasing SiO_2 [101].

According to Loucks [101], the effect of increasing water content in a melt promotes the crystallisation of hornblende well ahead of magnetite. The Sc concentration in porphyry Cu-forming magmas typically ranges between 3 and 8 ppm, yielding V/Sc ratios

of 10 to >15. V-Sc data for Duck Creek and Highway are shown in Figure 22a,c,d. These show a fractionation trend typical of reduced mafic and ultramafic magmas caused by olivine fractionation in the ferrogabbroic intrusion that hosts the Duck Creek mineral system. However, at low Sc concentrations, Duck Creek lithologies, and to some extent Highway lithologies, both develop a trend to very high V/Sc ratios, like those seen in Cu-Au porphyries (Figure 22e). Thus, the Duck Creek mineral system has clearly evolved from highly reduced source magmas to strongly oxidised porphyry magmas, like Grasberg, Northparkes and Cadia. Importantly, several of deposits in the eastern Mount Isa Block (Figure 22f), including Elaine Dorothy at Mary Kathleen (Figure 22b), interpreted as IOCG deposits, also define a mixing-trends that indicate evolution from reduced primary source magmas to strongly oxidised evolved magmas.

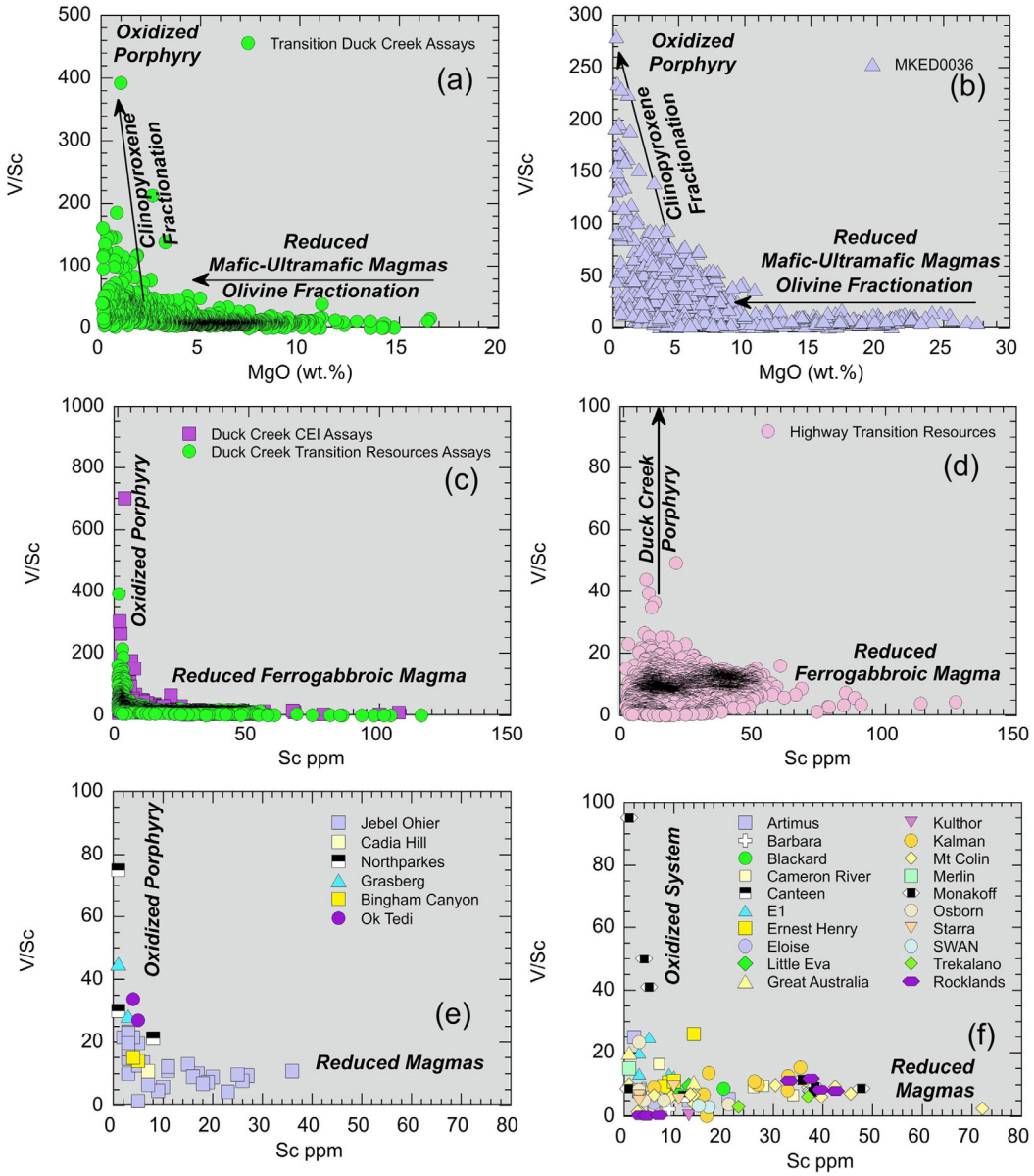


Figure 22. (**a**,**c**,**d**) V-Sc systematics of Duck Creek and Highway showing a fractionation trend typical of reduced mafic and ultramafic magmas caused by olivine fractionation in the ferrogabbroic source intrusion that hosts the Duck Creek mineral system. At low Sc concentrations, Duck Creek lithologies and to some extent Highway lithologies evolve to high V/Sc ratios, (**e**) shows V-Sc systematics in Cu-Au porphyries. (**b**,**f**) V-Sc systematics of so-called IOCG deposits in the eastern Mount Isa Block, including Elaine Dorothy.

5.1.6. Trace Element Vectors Indicating Tectonic Setting and Role of Sulphate Fractionation

Multi-element ratio Nb/Y versus Nb + Y plots for samples from the Highway–Duck Creek mineral system are shown in Figure 23a–c. Also shown in Figure 23c are data from Elaine Dorothy. Figure 23d shows data for Jebel Ophier (Saudi Arabia), Bingham Canyon, Porgera and Northparkes Cu-Au porphyry deposits, and Figure 23e shows data for several of the so-called IOCG deposits in the eastern Mount Isa Block.

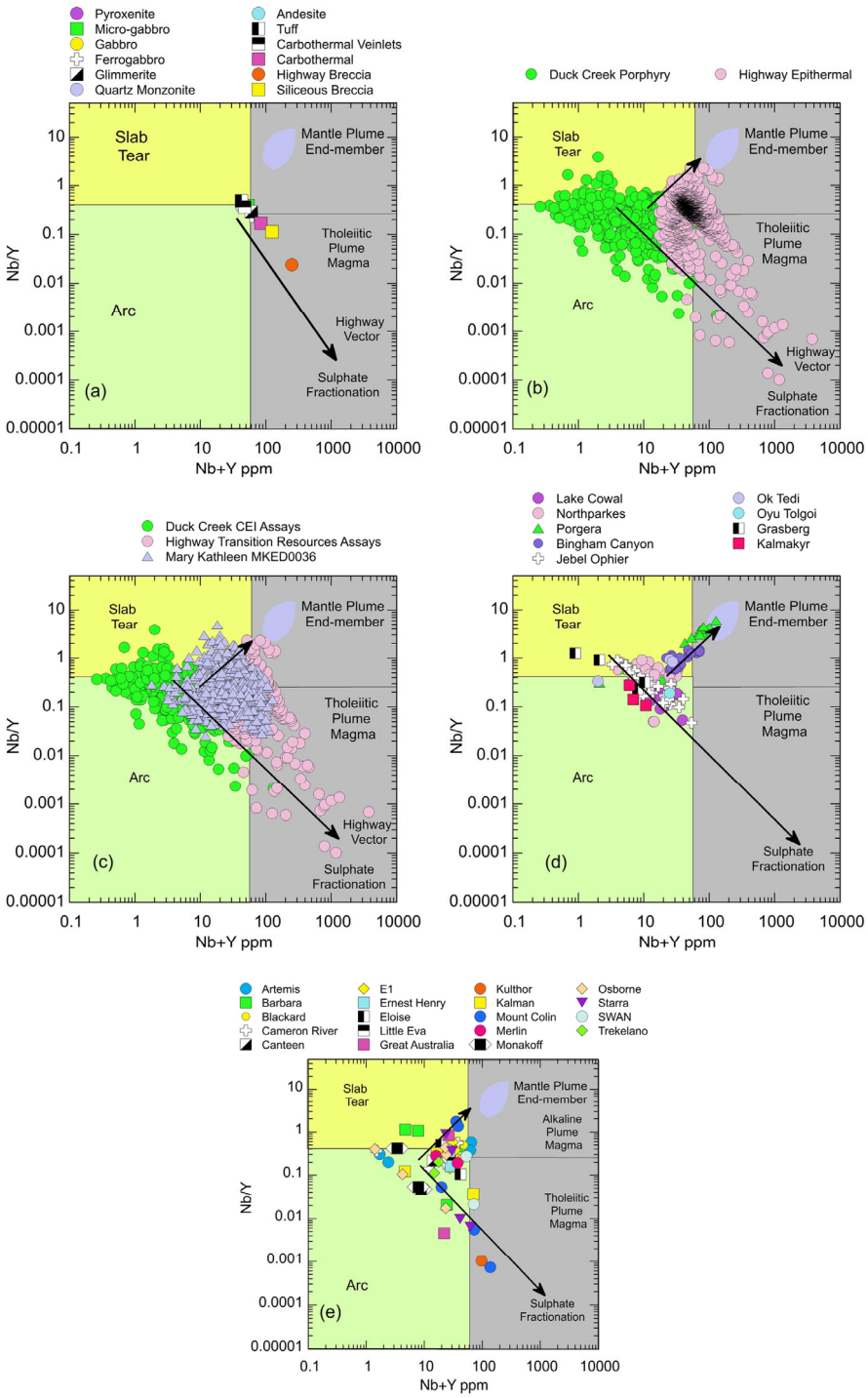


Figure 23. Multi-element plots showing Nb/Y versus Nb + Y systematics, showing (**a**) Highway lithologies, (**b**) Highway and Duck Creek data, (**c**) comparison between Highway–Duck Creek and Elaine Dorothy deep MKED0036 core, (**d**) comparative data for selected Cu-Au porphyries, (**e**) Cloncurry "IOCG" systems. All show the impact of sulphate fractionation, leading to an increase in Y (HREE) concentrations.

This plot, initially developed by Whelan and Hildebrand [102], allows discrimination between tectonic settings, i.e., Slab Tear, Magmatic Arc and Mantle Plume. In Figure 23a–c, samples from Highway and Duck Creek mineral systems plot in the slab tear and magmatic arc fields (Slab Window), with a subtle vector towards the mantle plume field. Both Highway and Duck Creek systems define a vector that extends into the right-hand bottom quadrant of the diagram with very low Nb/Y and high Nb + Y values caused by enrichment in Y, caused by sulphate–fluid fractionation that involved REE-SO_2- complexing [103,104].

The Highway–Duck Creek deposits are interpreted to have evolved via magmatic–hydrothermal processes from a deep porphyry to a shallow epithermal environment. The system exhibits a definitive phyllic, propylitic and potassic alteration halo. The metallogenic process initially involved crystallisation of reduced potassic ultramafic to intermediate (pyroxenites–gabbros–monzogabbros) magmas that evolved to oxidised magmas saturated with metal-rich aqueous fluids. The final stage of the mineralisation event was controlled by sulphate reduction that was likely initiated by magnetite crystallisation. This caused a decrease in pH and also in the oxidation potential of sulphate, resulting in substantial fractionation of Y from Nb and leading to the enrichment in the HREEs seen at Highway (Figure 23). In this regard, it is significant that the most REE-enriched Highway samples have the highest S contents (Table 1).

5.1.7. Variation in Molar Cu/Au with Depth

Molar Cu/Au ratios and bulk metal contents, specifically Au grades in porphyry deposits are interpreted to be controlled by magmatic chemistries [104–106] and by fluid phase separation into brine and vapour, resulting in Cu-Au fractionation into a vapour phase and possibly to partial separation of the two metals [105–109]. However, ore grades are ultimately controlled by the precipitation efficiency of Cu-sulphides and native Au during cooling [110].

A positive correlation between the Cu/Au ratio and depth has been demonstrated [111–115]. However, magma source is not the sole factor determining the bulk metal ratio of the deposits, and according to Murakami et al. [116], the systematic variation of molar Au/Cu ratios of porphyry-style ore deposits with depth is related to the density evolution of cooling magmatic hydrothermal fluids. This is because fluid pressure controls the extent of fluid phase separation into brine and vapour, causing fractionation of ore-forming components. In addition, fluid density evolution, together with temperature, also affects the differential solubility and selective precipitation of ore minerals. Thus, molar Cu/Au ratios are controlled initially by magma source chemistries and subsequently by depth, where the physical–chemical evolution of the ore-forming hydrothermal fluids occurred.

Figure 24 shows that molar Cu/Au ratios for samples, obtained by reverse-circulation drilling versus depth, exhibit an increase in molar Cu/Au ratios from ~10 to 100,000 in the Highway area (east) through "Comway" to between 200,000 and 10,000,000 in the Duck Creek (west) system. This supports the exploration model that the Highway system is a shallow Au-dominated epithermal system, and Duck Creek is a deeper Cu-Au-bearing porphyry. The "Comway" deposits lie between Highway and Duck Creek at an intermediate crustal depth, with molar Cu/Au ratios between 60,000 and ~120,000, typical of alkaline porphyry systems, to a deeper Cu-dominated porphyry system at Duck Creek with ratios up to ~2,000,000. Note a near-surface sample from Success with a molar Cu/Au of ~80,000,000 is Cu enriched due to supergene alteration.

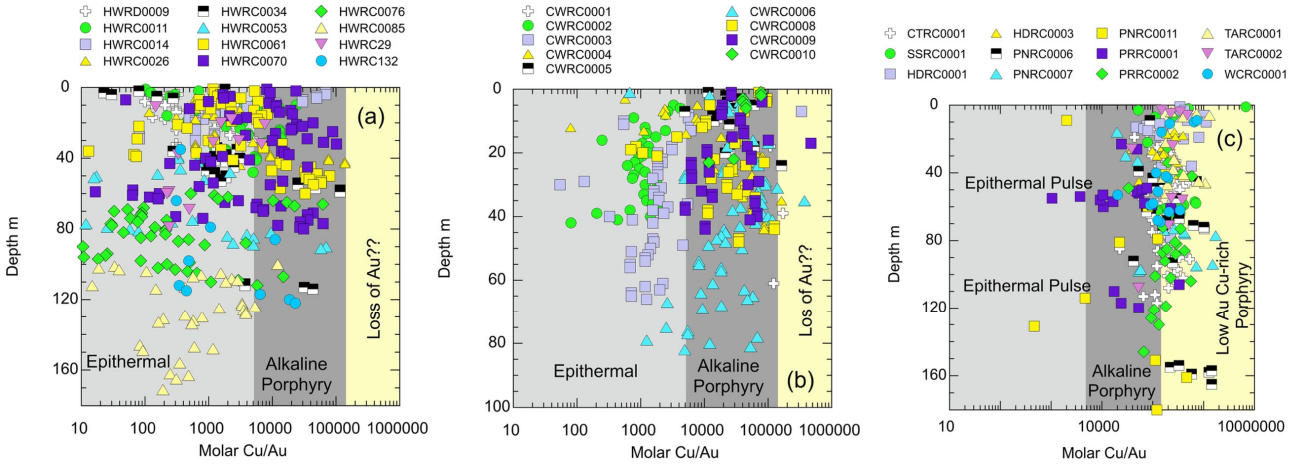


Figure 24. Plots showing molar Cu/Au ratio versus depth in a crustal transect from shallow at High-way to deep at Duck Creek. The data show an increase in molar Cu/Au with depth from the (**a**) east (Highway) to the (**c**) west (Duck Creek). (**b**) Comway lies between Highway and Duck Creek at an intermediate crustal dept. This figure provides further support to the exploration model that the Highway system is a shallow Au-dominated epithermal system, and Duck Creek is a deeper Cu-Au-bearing porphyry. Comway with molar Cu/Au ratios between 60,000 and ~120,000, typical of alkaline porphyry systems. The deeper Cu-dominated porphyry system at Duck Creek, has molar Cu/Au ratios up to ~2,000,000. Note a near-surface sample from Success with a molar Cu/Au of ~80,000,000 is Cu-enriched due to supergene alteration.

5.1.8. Nb/Ta Ratios and the Role of a Mantle Component in NWMP Mineralisation

The Nb and Ta are "twin elements", with identical charge (+5) and almost identical ionic size, which do not generally fractionate during the partial melting. The Nb/Ta ratio of the depleted mantle and the continental crust is assumed to be geochemically complementary reservoirs. However, the Nb/Ta ratio of the continental crust ranges from 10 to 12 [117,118], and the Nb/Ta ratio in the depleted (upper) mantle is 15.5 [119]. These are significantly less than the chondritic value of 19 [120]. Thus, mixtures of depleted upper mantle and continental crust do not produce the chondritic Nb/Ta ratios and balance the primitive mantle [120]. This indicated that another geochemical reservoir with superchondritic Nb/Ta is required to balance the low Nb/Ta observed in the continental crust. Kamber and Collerson [119] showed that fractionation of the chemical twins Nb and Ta can occur by dehydration during the subduction of oceanic lithosphere. Melting associated with this process produced arc lavas and continental crust with a low Nb/Ta ratio, leaving an eclogitic residue with a superchondritic Nb/Ta ratio. Kamber et al. [118] have shown that weathered continental crust represented by alluvial sediments derived from Precambrian to Tertiary crust has an average Nb/Ta ratio of 9.76, indicating that the crustal low Nb/Ta ratio is an extremely robust value.

The Nb/Ta ratio is a useful vector to discriminate between metallogenic crustal and mantle sources, as Nb and Ta do not fractionate during crustal partial melting. This is particularly true for lithologies associated with deep-sourced mantle plumes that originate from the Earth's primitive lower mantle, e.g., kimberlites with Nb/Ta of 17.9 to 23 [11] and oceanic carbonatites with Nb/Ta ranging from 32 to 474 [121,122]. Nb/Ta ratios of >~17 exhibited by ocean island basalt (both EM1 "enriched mantle" and "HIMU" end-members) are also interpreted to reflect their lower mantle primitive source compositions [11]. Alternative models for the location of the high Nb/Ta reservoir include the subcontinental lithospheric mantle [44], possibly containing melts derived from subducted carbonate [123] or in Earth's core [124].

Many of the Cloncurry area "IOCG" deposits, e.g., E1, Monakoff, Merlin, Eloise, etc., and the Highway–Duck Creek mineral system exhibit superchondritic Nb/Ta ratios (Figure 25). The "IOCG" deposits are spatially associated with the Williams and Naraku batholith (1545–1490 Ma), a suite of intrusions that is interpreted to be the primary source of metals in these deposits. However, this is unlikely, as Williams Batholith intrusions, e.g., Wimberu Granite, Saxby Granite, Wiley Granite, Mount Anglesay Granite and the Squirrel Hill Granite all exhibit subchondritic Nb/Ta ratios <10. Whereas, the "IOCG" deposits all have significantly higher Nb/Ta ratios, well above the average Nb/Ta ratio (Nb/Ta 10–12) of continental crust [117,118].

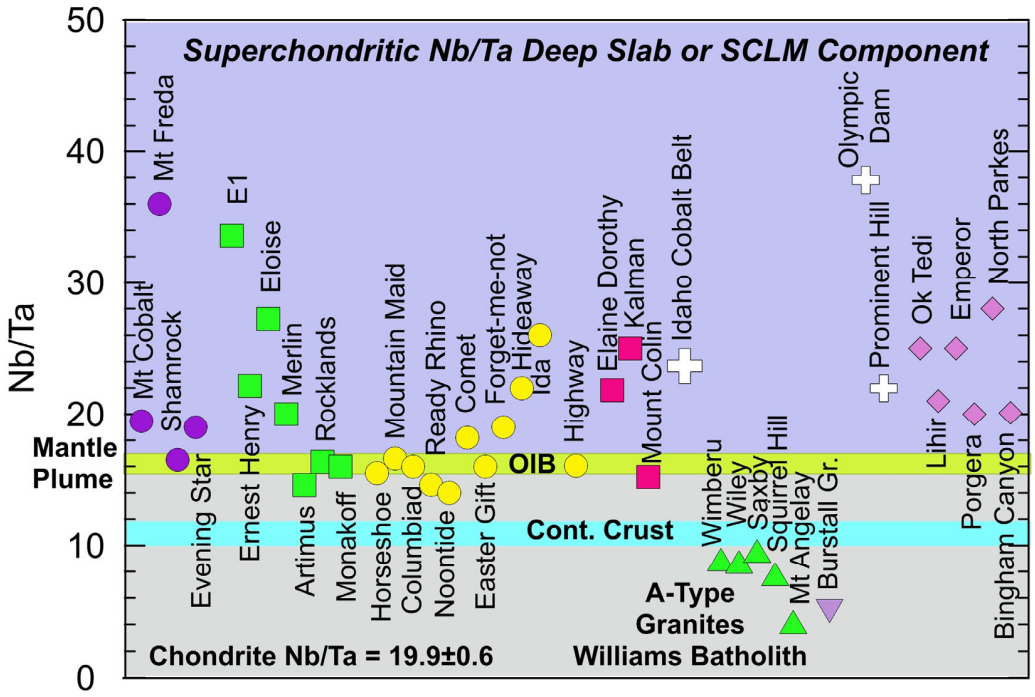


Figure 25. Nb/Ta ratio variability in NWMP deposits and Williams Batholith postulated sources. Also shown for comparison, average Nb/Ta ratios of porphyry deposits, Olympic Dam and Prominent Hill IOCG deposits and REE-rich Co ores from the Idaho Cobalt Belt. Sources of data: Highway (Table 1); Duck Creek deposits (Table 2); NWMP deposits—Shamrock, Evening Star, Mt Freda (Collerson 2019), Ernest Henry, Artimus, E1, Monakoff, Eloise, Rocklands, Merlin (OSNACA data [82]; Elaine Dorothy [46]; Wimberu Granite [63]; Continental Crust [115,116]; Chondrite Nb/Ta [120]; Squirrel Hill [125]; Mt. Angelay granite [126]; Saxby and Wiley granite [126]; Mount Cobalt Idaho Cobalt Belt [127]; Ocean Island Basalt–Mantle Plume [11].

The high Nb/Ta ratio of these deposits shows that metals in this system were clearly not derived from a low Nb/Ta crustal source. The Sc, Ni, Co, Pd and Pt tenor of many of these deposits supports the interpretation of mantle-derived melts, like the potassic ultramafic–intermediate pyroxenitic–gabbroic–monzogabbroic intrusions identified at Highway and Duck Creek. Several other domains characterised by elevated Nb/Ta ratios are present in the NWMP, e.g., at Mount Cobalt (average Nb/Ta ~25), Elaine Dorothy (average Nb/Ta ~48.6) and Lawlor (average Nb/Ta ~54), and it is likely that metals derived from such domains played a major role in post-collisional NWMP mineralisation. For example, calcium-rich alkaline lithologies from a deep diamond drill hole, MKED0036, between ~250 and 850 m, at Mary Kathleen. In these lithologies, CaO ranges from ~20 to 39 wt.%, Cu contents are up to 1.15 wt. %, and Ni, Co, U, Th and REEs range up to 890 ppm, 64 ppm, U 400 ppm, Th 2000 ppm and 1%, respectively.

From the almost ubiquitous high Nb/Ta ratio character of deposits in the eastern NWMP (Figure 25), it is likely that this previously unrecognised Ca-rich magmatic system played a role in Mesoproterozoic post-collisional metallogenesis in the area. These Ca-rich intrusions preserve igneous textures and are clearly post-tectonic and hence post-collisional. They are interpreted to represent part of an alkaline suite that is likely genetically associated with the tholeiitic ferrogabbros and monzogabbros, as seen in the Duck Creek system. As lithologies with elevated Nb/Ta ratios extend from Mary Kathleen to Mount Cobalt in the south and to Ernest Henry in the Northeast, this high Ca alkaline system is interpreted to underlie a large region of the eastern Mount Isa block.

This alkaline and tholeiite system is interpreted to have been emplaced through a palaeo-slab window that accreted to the eastern margin of the North Australian craton following Numil Terrane collision from the east (Figure 26). This collisional environment provided the geodynamic setting, the metal source and the plumbing system for the formation of post-collisional mineralisation in the Highway–Duck Creek area that exhibits all the hallmarks of a Cu-Au porphyry–epithermal mineral system. There are two major metal sources for this mineral system, one associated with tholeiitic ferrogabbros, and the other a high Ca alkaline system with high Nb/Ta ratios.

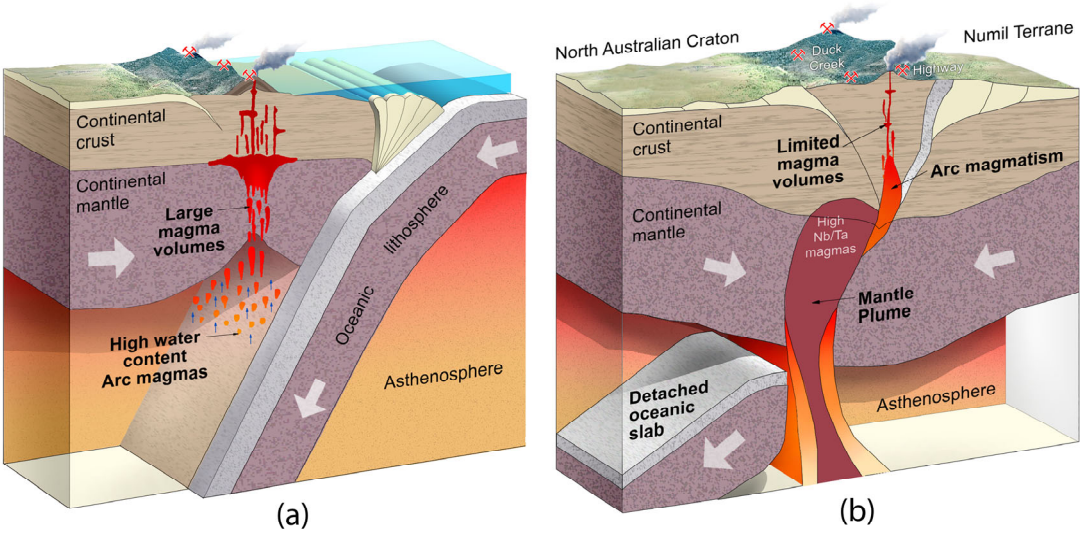


Figure 26. Schematic geodynamic cartoon comparing (**a**) subduction-generated Cu-Au porphyry systems, where metals are derived from subducting oceanic crust, with (**b**) post-tectonic collisional porphyry systems, where a slab window has allowed passage of a deep mantle upwelling that interacts with a high Nb/Ta slab (eclogite) located in the transition zone and upper lower mantle. The superchondritic Nb/Ta slab and the upwelling plume are additional metal sources for post-collisional porphyry that explain the presence of superchondritic Nb/Ta ratios, as well as elevated Pt and Pd chemistries.

A possible deep porphyry magnetic target has been imaged at a depth of ~1 km below the northern portion of the Highway epithermal system using sub-audio magnetics. If this magnetic anomaly extends for the entire length of the Highway epithermal system, viz., ~20 km (Figure 1), then based on the epithermal–porphyry model proposed in this paper, the Duck Creek Cu-Au porphyry clearly represents a major new Cu system discovery in the NWMP.

6. Summary and Conclusions

Lithological, geochemical and geodynamic models for the eastern margin of the north Australian craton all support the interpretation that the Highway–Duck Creek area hosts a

post-subduction collisional Cu-Au epithermal—porphyry mineral system. The Cu-poor epithermal system at Highway overlies Cu-Au porphyry mineralisation. Timing of mineralisation based on U-Pb, LA ICPMS geochronology of xenotime and monazite is between ~1490 and 1530 Ma. The epithermal Au-Te-W-REE mineralisation is hosted by siliceous breccias that show classic epithermal comb textures. Euhedral and subhedral crystals of quartz in carbothermal lithologies exhibit embayed grain boundaries that indicate acidic corrosion by F or B-rich fluids, as evidenced by the presence of tourmaline. Epithermal lithologies have high Au contents and low molar Cu/Au ratios of 6.16 g/t and 19 (epithermal breccia) and 3.46 g/t 475 (carbothermal lithologies), typical of epithermal systems. However, the underlying mafic intrusion and Marraba volcanic host rocks of Highway also have low, molar Cu/Au ratios, e.g., ferrogabbro (5571), quartz monzonite (4051) and andesite (680), with average Au concentrations ranging from 0.03 to 0.35 g/t. Gold occurs as native Au and as Au telluride. Bismuth is also enriched (24 ppm), occurring as Bi telluride. The occurrence of Au and Bi tellurides is typical of epithermal systems. Tungsten is hosted by wolframite and scheelite. REEs occur in xenotime and monazite, and thus the system is heavily REE-enriched. This heavy REE enrichment was caused by sulphate fractionation at a late stage of the fluid evolution of the system.

The two systems exhibit broadly uniform-shaped geochemical patterns, with positive spikes in W, U, Pb, P and Li and negative spikes in Ba, Th, Nb, Ta and Sr. The pronounced depletion in Sr, a common feature seen at both Duck Creek and Highway, is interpreted to have been caused by the breakdown of Ca-Sr-bearing minerals during pervasive phyllic, argillic, propylitic and potassic alteration associated with the porphyry mineralisation. Highway also shows a pronounced negative Ti spike, which is not seen at Duck Creek, suggesting the fractionation of a Ti-bearing mineral into the gabbro–monzogabbro intrusion, which was the source of the epithermal fluids. Although the level of W enrichment in all Highway lithologies is significantly greater than at Duck Creek, the patterns are broadly similar, with relatively consistent immobile-incompatible element ratios. These parallel profiles at Duck Creek and Highway support the view that they are related systems and that metals in the Highway epithermal system were delivered by fluids derived from the deeper Duck Creek post-tectonic potassic intrusive suite.

The Cu-Au-Ni-Co-Pt-Pd-Sc-rich porphyry is hosted by gabbro and norite, an association similar to other collisional orogen-hosted Cu-Au porphyry deposits, e.g., Beleuti, Akcha, Kalmakyr, Elasite, Assarel, Medet and Tsar Assen [97]. The Duck Creek porphyry sulphides are characterised by an assemblage of early crystallised pyrite, followed by chalcopyrite and bornite formed by hydrothermal alteration of the chalcopyrite. Cu sulphides also show the effect of supergene oxidation alteration, producing rims of covellite, chalcocite and digenite.

Redox conditions deduced from the V/Sc systematics show that the Duck Creek porphyry system contains both oxidised (typical of porphyries) and reduced source lithologies. Covariation plots of Ni/Te and Cu/Te show that Highway epithermal lithologies and Duck Creek porphyry lithologies clearly plot within the definitive fields of comparative global mineral system data sets. Chalcophile and highly siderophile element (Cu, MgO and Pd) systematics show that there is a remarkable similarity between the compositions of Duck Creek samples with similar data from porphyry mineral systems, such as Cadia, Northparkes, Bingham Canyon, Grasberg, Skouries, Kalmakyr, Elaisite, Assarel and Medet.

Geochemical vectors indicate that the Highway epithermal and Duck Creek porphyry systems involved three metal sources, viz., tholeiitic ferrogabbro, potassic ultramafic to mafic and Fe and Ca-rich alkaline. The latter two sources imparted the high Nb/Ta ratios that characterise many of the deposits. These alkaline and tholeiite systems are interpreted to be genetically associated with an upwelling thermochemical plume that

penetrated a palaeo-slab window that had accreted to the lithospheric mantle below the North Australian craton, following collision from the east by the Numil Terrane [48]. This collisional environment provided the geodynamic setting, the metal source and the plumbing system for the formation of post-collisional mineralisation in the Highway–Duck Creek area, with all the hallmarks of a Cu-Au porphyry–epithermal mineral system.

Author Contributions: Conceptualisation, K.D.C. and D.W.; methodology, K.D.C. and D.W.; formal analysis, K.D.C.; investigation, K.D.C.; resources, D.W.; data curation, D.W.; writing—original draft, K.D.C.; writing—review and editing, K.D.C. and D.W.; visualisation, K.D.C. and D.W.; supervision, K.D.C. and D.W.; project administration, D.W. All authors have read and agreed to the published version of the manuscript.

Funding: Research for this paper received some funding from the Queensland Department of Mines via a Collaborative Exploration Initiative Grant in 2000; however, the majority of funding was provided by shareholders of Transition Resources, who have strongly supported this exploration program.

Data Availability Statement: The raw data supporting the conclusions of this article will be made available by the authors on request.

Acknowledgments: We wish to acknowledge the contribution to this discovery made by Transition Resources' geological team, in particular, William Green, Enrico Scacchetti and Kevin Tidy. We also acknowledge the important input from three anonymous referees who have significantly improved the manuscript.

Conflicts of Interest: Author Kenneth David Collerson and David Wilson was employed by the company Transition Resources. The authors declare that the research was conducted in the absence of any commercial or financial relationships that could be construed as a potential conflict of interest.

References

1. Sillitoe, R.H. Porphyry copper systems. *Econ. Geol.* **2020**, *105*, 3–41.
2. Richards, J.P. Porphyry copper deposit formation in arcs: What are the odds? *Geosphere* **2021**, *18*, 130–155. [CrossRef]
3. Sillitoe, R.H. A plate tectonic model for the origin of porphyry copper deposits. *Econ. Geol.* **1972**, *67*, 184–197. [CrossRef]
4. Wilkinson, J.J. Triggers for the formation of porphyry ore deposits in magmatic arcs. *Nat. Geosci.* **2013**, *6*, 917–925. [CrossRef]
5. Lamont, T.N.; Loader, M.A.; Roberts, N.M.; Cooper, F.J.; Wilkinson, J.J.; Bevan, D.; Gorecki, A.; Kemp, A.; Elliott, T.; Gardiner, N.J.; et al. Porphyry copper formation driven by water-fluxed crustal melting during flat-slab subduction. *Nat. Geosci.* **2024**, *17*, 1306–1315. [CrossRef]
6. Hou, Z.; Yang, Z.; Lu, Y.; Kemp, A.; Zheng, Y.; Li, Q.; Tang, J.; Yang, Z.; Duan, L. A genetic linkage between subduction-and collision-related porphyry Cu deposits in continental collision zones. *Geology* **2015**, *43*, 247–250. [CrossRef]
7. Wang, Z.; Zheng, Y.; Chiaradia, M.; Xu, B.; Hao, H.; Hou, Z. Divergent paradigms of porphyry copper deposits in subduction and collision zones. *Earth arXiv* **2025**. [CrossRef]
8. Collerson, K.; Lal, S.; Williams, Q.; Rost, S. Cracking the metallogenic code for Fijian epithermal gold mineralisation. In *Proceedings of the Extended Abstracts, Pacrim 2015 Congress*; PACRIM: Hong Kong, China, 2015; pp. 219–226.
9. Holm, R.J.; Tapster, S.; Jelsma, H.A.; Rosenbaum, G.; Mark, D.F. Tectonic evolution and copper-gold metallogenesis of the Papua New Guinea and Solomon Islands region. *Ore Geol. Rev.* **2019**, *104*, 208–226. [CrossRef]
10. Ward, J.F.; Rosenbaum, G.; Ubide, T.; Sandiford, M. Slab segmentation, anomalous arc volcanism, and giant porphyry copper deposits in Indonesia. *Earth Planet. Sci. Lett.* **2024**, *626*, 118532. [CrossRef]
11. Collerson, K.D.; Williams, Q.; Ewart, A.E.; Murphy, D.T. Origin of HIMU and EM-1domains sampled by ocean island basalts, kimberlites and carbonatites: The role of CO2-fluxed lower mantle melting in thermochemical upwellings. *Phys. Earth Planet Int.* **2010**, *181*, 112–131. [CrossRef]
12. Tarkian, M.; Hünken, U.; Tokmakchieva, M.; Bogdanov, K. Precious-metal distribution and fluid-inclusion petrography of the Elatsite porphyry copper deposit. *Bulg. Miner. Depos.* **2003**, *38*, 261–281. [CrossRef]
13. Economou-Eliopoulos, M.; Eliopoulos, D.G. Palladium, platinum and gold concentration in porphyry copper systems of Greece and their genetic significance. *Ore Geol. Rev.* **2000**, *16*, 59–70. [CrossRef]
14. Economou-Eliopoulos, M. Exploration for Deposits of Platinum-Group Elements. *Miner. Assoc. Can. Short Course* **2005**, *35*, 203–246.

15. Economou-Eliopoulos, M. Platinum-group elements (PGE) in various geotectonic settings: Opportunities and risks. *Hell. J. Geosci.* **2010**, *45*, 65–82.
16. Economou-Eliopoulos, M.; Zaccarini, F.; Garuti, G. Fertility indicators for porphyry-Cu- Au+Pd±Pt deposits: Evidence from Skouries, Chalkidiki Peninsula, Greece, and comparison with worldwide mineralizations. *Minerals* **2023**, *13*, 1413. [CrossRef]
17. Sun, W.; Huang, R.-F.; Li, H.; Hu, Y.-B.; Zhang, C.-C.; Sun, S.-J.; Zhang, L.-P.; Ding, X.; Li, C.-Y.; Zartman, R.E.; et al. Porphyry deposits and oxidized magmas. *Ore Geol. Rev.* **2015**, *65*, 97–131. [CrossRef]
18. Yuan, F.; Zhou, T.; Zhang, D.; Jowitt, S.M.; Keays, R.; Liu, S.; Fan, Y. Siderophile and chalcophile metal variations in basalts: Implications for the sulphide saturation history and Ni–Cu–PGE mineralization potential of the Tarim continental flood basalt province, Xinjiang Province, China. *Ore Geol. Rev.* **2012**, *45*, 5–15. [CrossRef]
19. Li, J.; Liu, W.; Su, L.; Li, D.; Zhang, S.; Chen, H. Porphyry copper mineralization triggered by sulfate reduction and alkali metasomatism: Constraints from an experimental investigation. *GSA Bull.* **2023**, *135*, 2407–2427. [CrossRef]
20. Kesler, S.E.; Wilkinson, B.H. The role of exhumation in the temporal distribution of ore deposits. *Econ. Geol.* **2006**, *101*, 919–922. [CrossRef]
21. Simmons, S.F.; White, N.C.; John, D.A. Geological characteristics of epithermal precious and base metal deposits. In *Economic Geology*; Hedenquist, J.W., Thompson, J.F.H., Goldfarb, R.J., Richards, J.P., Eds.; Society of Economic Geologists: Littleton, CO, USA, 2005; Volume 100, pp. 485–522.
22. Sillitoe, R.H. Epithermal paleosurfaces. *Miner. Depos.* **2015**, *50*, 767–973. [CrossRef]
23. Dong, G.; Morrison, G.; Jaireth, S. Quartz textures in epithermal veins, Queensland: Classification, origin and implication. *Econ. Geol.* **1995**, *90*, 1841–1856. [CrossRef]
24. Groves, D.I.; Bierlein, F.P.; Meinert, L.D.; Hitzman, M.W. Iron oxide-copper-gold (IOCG) deposits through Earth History: Implications for origin, lithospheric setting and distinction from other epigenetic iron oxide deposits. *Econ. Geol.* **2010**, *105*, 641–654. [CrossRef]
25. Kalinin, A.A.; Kudryashov, N.M. Porphyry-related metamorphosed Au-Ag and Cu-Mo Deposits in the Precambrian of the Fennoscandian Shield. *Minerals* **2021**, *11*, 139. [CrossRef]
26. Marshall, A.E. *Low Temperature-Low Pressure ("Epithermal") Siliceous Vein Deposits of the North Pilbara Granite-Greenstone Terrane, Western Australia*; Australian Geological Survey Organisation Record: Canberra, Australia, 2000.
27. McCuaig, T.C.; Behn, M.; Stein, H.; Hagemann, S.G.; McNaughton, N.J.; Cassidy, K.F.; Champion, D.C.; Wyborn, L. The Boddington gold mine: A new style of Archaean Au-Cu deposit. *Geosci. Aust. Rec.* **2001**, *37*, 453–455.
28. Lopes, A.A.C.; Moura, M.A. Gold Deposit, Tapajós Mineral Province (Brazil): Geology, Petrology and Fluid Inclusion Evidence for Ore-Forming Processes. *Minerals* **2019**, *9*, 29. [CrossRef]
29. Mumin, A.H.; Somarin, A.K.; Jones, B.; Corriveau, L.; Ootes, L.; Camier, J. The IOCG- porphyry-epithermal continuum of deposit types in the Great Bear magmatic zone, North- west Territories, Canada. In *Exploring for Iron Oxide Copper-Gold Deposits: Canada and Global Analogues. Geological Association of Canada Short Course Notes*; Corriveau, L., Mumin, H., Eds.; Geological Association of Canada (GAC): St. John's, NL, Canada, 2020; Volume 20, pp. 59–78.
30. Richards, J.P.; Mumin, A.H. Magmatic-hydrothermal processes within an evolving Earth: Iron oxide-copper-gold and porphyry Cu ± Mo ± Au deposits. *Geology* **2013**, *41*, 767–770. [CrossRef]
31. Tiddy, C.J.; Giles, D. Suprasubduction model for metal endowment at 1.60–1.57 Ga in eastern Australia. *Ore Geol. Rev.* **2020**, *122*, 103483. [CrossRef]
32. Tornos, F.; Velasco, F.; Barra, F.; Morata, D. The Tropezón Cu–Mo–(Au) deposit, Northern Chile: The missing link between IOCG and porphyry copper systems? *Miner. Depos.* **2010**, *45*, 313–321. [CrossRef]
33. Sillitoe, R.H. Iron oxide–copper–gold deposits: An Andean view. *Miner. Depos.* **2003**, *38*, 787–812. [CrossRef]
34. Brauhart, C.W.; Groves, D.I. Australian intracratonic copper-gold and allied deposits: A clan of mineral systems. *Ore Geol. Rev.* **2025**, *149*, 158–182. [CrossRef]
35. Williams, P.; Barton, M.D.; Johnson, D.A.; Fontboté, L.; Ad, H.; Mark, G.; Oliver, N.H.S.; Marschik, R. Iron oxide copper–gold deposits: Geology, space–time distribution, and possible modes of origin. In *Economic Geology*; Hedenquist, J.W., Thompson, J.F.H., Goldfarb, R.J., Richards, J.P., Eds.; Society of Economic Geologists: Littleton, CO, USA, 2005; Volume 100, pp. 371–406.
36. Gibson, G.M.; Meixner, A.J.; Withnall, I.W.; Korsch, R.J.; Hutton, L.J.; Jones, L.E.A.; Holzschuh, J.; Costelloe, R.D.; Henson, P.A.; Saygin, E. Basin architecture and evolution in the Mount Isa mineral province, northern Australia: Constraints from deep seismic reflection profiling and implications for ore genesis. *Ore Geol. Rev.* **2016**, *76*, 414–441. [CrossRef]
37. Pollard, P.J. An intrusion-related origin for Cu- Au mineralization in iron oxide-copper-gold (IOCG) provinces. *Miner. Depos.* **2006**, *4*, 179–187. [CrossRef]
38. Baker, T. Alteration, mineralisation and fluid evolution at the Eloise Cu—Au deposit, Cloncurry district, NW Queensland. *Econ. Geol.* **1998**, *93*, 1213–1236. [CrossRef]
39. Mark, G.; Oliver, N.H.S.; Carew, M.J. Insights into the genesis and diversity of epigenetic Cu—Au mineralisation in the Cloncurry district. Mt Isa Inlier, northwest Queensland. *Aust. J. Earth Sci.* **2006**, *53*, 109–124. [CrossRef]

40. Williams, P.J.; Dong, G.; Ryan, C.G.; Pollard, P.J.; Rotherham, J.; Mernagh, T.P.; Chapman, I.H. Geochemistry of hypersaline fluid inclusions from the Starra (Fe oxide)—Cu—Au deposit, Cloncurry district, Queensland. *Econ. Geol.* **2001**, *96*, 875–884.
41. Marshall, L.J.; Oliver, N.H.S. Constraints on hydrothermal fluid pathways within Mary Kathleen Group stratigraphy of the Cloncurry iron-oxide–copper–gold District, Australia. *Precambrian Res.* **2008**, *163*, 151–158. [CrossRef]
42. Collerson, K.D. *Cobalt and HREE Mineral Systems in the Mount Isa Block*; Report for Geological Survey of Queensland; Geological Survey of Queensland: Brisbane, Australia, 2018. Available online: https://geoscience.data.qld.gov.au/report/cr111110.
43. Weidendorfer, D.; Schmidt, M.X.; Mattsson, H.B. Fractional crystallization of Si-undersaturated alkaline magmas leading to unmixing of carbonatites on Brava Island (Cape Verde) and a general model of carbonatite genesis in alkaline magma suites. *Contrib. Miner. Petrol.* **2016**, *171*, 43. [CrossRef]
44. Pfänder, J.A.; Jung, S.; Münker, C.; Stracke, A.; Mezger, K. A possible high Nb/Ta reservoir in the continental lithospheric mantle and consequences on the global Nb budget-Evidence from continental basalts from Central Germany. *Geochim. Cosmochim. Acta* **2012**, *77*, 232–251. [CrossRef]
45. Tang, M.; Lee, C.-T.A.; Chen, K.; Erdman, M.; Costin, G.; Jiang, H. Nb/Ta systematics in arc magma differentiation and the role of arclogites in continent formation. *Nat. Commun.* **2019**, *10*, 235. [CrossRef]
46. Collerson, K.D. *Core Lithologies from Elaine Dorothy and Blue Caesar Prospects: A Geochemical Interpretation based on Assays From Elaine Dorothy, Mary Kathleen Belt, North Queensland*; Report for China Yunnan Copper Resources Ltd.; HDR Salva: Omaha, NE, USA, 2013; p. 95.
47. Wilson, I.H. Volcanism on a Proterozoic continental margin in northwestern Queensland. *Precambrian Res.* **1978**, *7*, 205–235. [CrossRef]
48. Korsch, R.J.; Huston, D.L.; Henderson, R.A.; Blewett, R.S.; Withnall, I.W.; Fergusson, C.L.; Collins, W.J.; Saygin, E.; Kositcin, N.; Meixner, A.J.; et al. Crustal architecture and geodynamics of North Queensland, Australia: Insights from deep seismic reflection profiling. *Tectonophysics* **2012**, *572*, 76–99. [CrossRef]
49. Korsch, R.J.; Doublier, M.P.; Brown, D.D.; Simpson, J.M.; Cross, A.J.; Ross, D.; Costelloe, R.D.; Jiang, W. Crustal architecture and tectonic development of western Queensland, Australia, based on deep seismic reflection profiling: Implications for Proterozoic continental assembly and dispersal. *Tectonophysics* **2024**, *878*, 230302. [CrossRef]
50. Betts, P.G.; Giles, D.; Schaefer, B.F.; Mark, G. 1600–1500 Ma hotspot track in eastern Australia: Implications for Mesoproterozoic continental reconstructions. *Terra Nova* **2007**, *19*, 496–501. [CrossRef]
51. Betts, P.G.; Giles, D.; Foden, F.; Schaefer, B.F.; Mark, G.; Pankhurst, M.J.; Caroline Forbes, C.J.; Williams, H.A.; Chalmers, N.C.; Hills, Q. Mesoproterozoic plume-modified orogenesis in eastern Precambrian Australia. *Tectonophysics* **2009**, *28*, TC3006. [CrossRef]
52. Gibson, G.M.; Champion, D.C.; Huston, D.L.; Withnall, I.W. Orogenesis in Paleo-Mesoproterozoic eastern Australia: A response to Arc–Continent and Continent–Continent Collision During Assembly of the Nuna Supercontinent. *Tectonics* **2020**, *39*, E2019TC005717. [CrossRef]
53. Li, J.; Song, X. Tearing of Indian mantle lithosphere from high-resolution seismic images and its implications for lithosphere coupling in southern Tibet. *Proc. Natl. Acad. Sci. USA* **2018**, *115*, 8296–8300. [CrossRef] [PubMed]
54. Rosenbaum, G.; Gasparon, M.; Lucente, F.P.; Peccerillo, A.; Miller, M.S. Kinematics of slab tear faults during subduction segmentation and implications for Italian magmatism. *Tectonics* **2008**, *27*, TC2008. [CrossRef]
55. Momme, P.; Oskarsson, N.; Keays, R.R.; Horan, M.F.; Brandon, A.D.; Neal, C.R. Platinum- group elements in the Icelandic rift system; melting processes and mantle sources beneath Iceland. *Chem. Geol.* **2003**, *196*, 209–234. [CrossRef]
56. Webber, A.P.; Roberts, S.; Taylor, R.N.; Pitcairn, I.K. Golden plumes: Substantial gold enrichment of oceanic crust during ridge-plume interaction. *Geology* **2013**, *41*, 187–190. [CrossRef]
57. Williams, P.R. Nature and timing of early extensional structures in the Mitakoodi Quartzite, Mount Isa Inlier, north- west Queensland. *Aust. J. Earth Sci.* **1989**, *36*, 283–296. [CrossRef]
58. Potma, W.A.; Betts, P.G. Extension-related structures in the Mitakoodi Culmination: Implications for the nature and timing of extension, and effect on later shortening in the eastern Mt Isa Inlier. *Aust. J. Earth Sci.* **2006**, *53*, 55–67. [CrossRef]
59. Skirrow, R.G. Iron oxide copper-gold (IOCG) deposits A review (Part 1): Settings, mineralogy, ore geochemistry and classification. *Ore Geol. Rev.* **2022**, *140*, 104569. [CrossRef]
60. MacCready, T.; Goleby, B.R.; Goncharov, A.; Drummond, B.J.; Lister, G.S. A framework of overprinting orogens based on interpretation of the Mount Isa deep seismic transect. *Econ. Geol.* **1989**, *93*, 1422–1434. [CrossRef]
61. O'Dea, M.G.; Betts, P.G.; MacCready, T.; Aillères, L. Sequential development of a mid-crustal fold-thrust complex: Evidence from the Mitakoodi Culmination in the eastern Mt. Isa Inlier, Australia. *Aust. J. Earth Sci.* **2006**, *53*, 69–90. [CrossRef]
62. Neumann, N.L.; Gibson, G.M.; Southgate, P.N. New SHRIMP age constraints on the timing and duration of magmatism and sedimentation in the Mary Kathleen Fold Belt, Mt Isa Inlier, Australia. *Aust. J. Earth Sci.* **2009**, *56*, 965–983. [CrossRef]
63. Hackenberg, O. The Wimberu Granite: Granitic Phases, Geochemistry, Geochronology and Thermobarometry. Bachelor's Thesis, University of Queensland, Queensland, Australia, 2018.

64. Zheng, Y.Y.; Chen, X.; Palmer, M.R.; Zhao, K.D.; Hernández-Uribe, D.; Gao, S.; Wu, S. Magma mixing and magmatic-to-hydrothermal fluid evolution revealed by chemical and boron isotopic signatures in tourmaline from the Zhunuo-Beimulang porphyry Cu-Mo deposits. *Miner. Depos.* **2024**, *59*, 1133–1153. [CrossRef]
65. Clark, R.; Smith, D.J.; Naden, J.; Holwell, D.; Mann, S. Mineralogical constraints on the genesis of an alkalic-type epithermal Au-Te deposit: Tuvatu, Fiji. *Ore Geol. Rev.* **2023**, *154*, 105279. [CrossRef]
66. Ryan, B. The Nain-Churchill Boundary and the Nain Plutonic Suite: A Regional Perspective on the Geologic Setting of the Voisey's Bay Ni-Cu-Co Deposit. *Econ. Geol.* **2000**, *95*, 703–724.
67. Baksheev, I.A.; Prokofev, V.Y.; Zaraisky, G.P.; Chitalin, A.F.; Yapaskurt, V.O.; Nikolaev, Y.N.; Kononov, O.V. Tourmaline as a prospecting guide for the porphyry-style deposits. *Eur. J. Miner.* **2012**, *24*, 957–979. [CrossRef]
68. Wallace, C.J.; Maher, K.C. Phyllic alteration and the implications of fluid composition at the Copper Flat hydrothermal System, New Mexico, USA. *Ore Geol. Rev.* **2019**, *104*, 273–293. [CrossRef]
69. Zhao, J.; Brugger, J.; Chen, G.; Ngothai, Y.; Pring, A. Experimental study of the formation of chalcopyrite and bornite via the sulfidation of hematite: Mineral replacements with a large volume increase. *Am. Mineral.* **2014**, *99*, 343–354. [CrossRef]
70. Reich, M.; Deditius, A.; Chryssoulis, S.; Li, J.-W.; Ma, C.-Q.; Parada, M.A.; Barra, F.; Mittermayr, F. Pyrite as a record of hydrothermal fluid evolution in a porphyry copper system: A SIMS/EMPA trace element study. *Geochim. Cosmochim. Acta* **2013**, *104*, 42–62. [CrossRef]
71. Philpott, R.C. Geology and Geochemistry of the Mount Cobalt Co-Cu-Au-REE IOCG Deposit, Cloncurry District, Queensland. Bachelor's Thesis, Monash University, Melbourne, Australia, 2010.
72. Peccerillo, A.; Taylor, S.R. Geochemistry of Eocene calk-alkaline volcanic rocks from the Kastamonu area, northern Turkey. *Contrib. Miner. Petrol.* **1976**, *58*, 63–81. [CrossRef]
73. Hastie, A.R.; Kerr, A.C.; Pearce, J.A.; Mitchell, S.F. Classification of Altered Volcanic Island Arc Rocks using Immobile Trace Elements: Development of the Th-Co Discrimination Diagram. *J. Petrol.* **2007**, *48*, 2341–2357. [CrossRef]
74. Mathieu, L. Quantifying Hydrothermal Alteration: A Review of Methods. *Geosciences* **2019**, *8*, 245. [CrossRef]
75. Muller, D.; Groves, D.I. *Potassic Igneous Rocks and Associated Gold-Copper Mineralization*, 5th ed.; Springer: Berlin/Heidelberg, Germany, 2019; p. 398.
76. Soder, C.G.; Dunga, J.; Romer, R.L. Continental subduction controls regional magma heterogeneity and distribution of porphyry deposits in post-collisional settings. *Geochim. Cosmochim. Acta* **2024**, *375*, 217–228. [CrossRef]
77. McDonough, W.F.; Sun, S.-S. The composition of the Earth. *Chem. Geol.* **1995**, *120*, 223–253. [CrossRef]
78. Lyubetskaya, T.; Korenaga, J. Chemical composition of the Earth's primitive mantle and its variance. *J. Geophys. Res.* **2007**, *112*, B03211.
79. Hikov, A. Geochemistry of strontium in advanced argillic alteration systems—Possible guide to exploration. *Bulg. Geol. Soc. Abtr. An. Sci. Confr.* **2004**, 29–31.
80. Hikov, A.; Lerouge, C.; Velinova, N. Geochemistry of alunite group minerals in advanced argillic altered rocks from the Asarel porphyry copper deposit, Central Srednogorie. *Rev. Bulg. Geol. Soc.* **2010**, *71*, 133–148.
81. Mavrogonatos, C.; Voudouris, P.; Spry, P.G.; Melfos, V.; Klemme, S.; Jasper Berndt, J.; Tim Baker, T.; Moritx, R.; Bissig, T.; Monecke, T.; et al. Mineralogical study of the advanced argillic alteration zone at the Konos Hill Mo–Cu–Re–Au Porphyry Prospect, NE Greece. *Minerals* **2018**, *8*, 479. [CrossRef]
82. Brauhart, C.W.; Grunsky, E.C.; Hagemann, S.G. Magmato-hydrothermal space: A new metric for geochemical characterisation of metallic ore deposits. *Ore Geol. Rev.* **2017**, *86*, 867–895. [CrossRef]
83. Rudnick, R.L.; Gao, S. Composition of the continental crust. In *The Crust*; Holland, H.D., Turekian, K.K., Eds.; Elsevier-Pergamon: Oxford, UK, 2003; pp. 1–64.
84. Holwell, D.A.; Fiorentini, M.; McDonald, I.; Lu, Y.; Giuliani, A.; Smith, D.J.; Keith, M.; Locmelis, M. A metasomatized lithospheric mantle control on the metallogenic signature of post-subduction magmatism. *Nat. Commun.* **2019**, *10*, 3511. [CrossRef]
85. Holwell, D.A.; McDonald, I. A review of the behaviour of platinum group elements within natural magmatic sulfide ore systems the importance of semimetals in governing partitioning behaviour. *Platin. Met. Rev.* **2010**, *54*, 26–36. [CrossRef]
86. Hoss, A.; Haase, K.M.; Keith, M.; Klemd, R.; Melfos, V.; Gerlach, L.; Pelloth, F.; Falkenberg, J.J.; Voudouris, P.; Strauss, H.; et al. Magmatic and hydrothermal evolution of the Skouries Au-Cu porphyry deposit, northern Greece. *Ore Geol. Rev.* **2024**, *173*, 106233. [CrossRef]
87. Grundler, P.V.; Brugger, J.; Etschmann, B.E.; Helm, L.; Liu, W.; Spry, P.G.; Pring, A. Speciation of aqueous tellurium(IV) in hydrothermal solutions and vapors, and the role of oxidized tellurium species in Te transport and gold deposition. *Geochim. Cosmochim. Acta* **2013**, *120*, 298–325. [CrossRef]
88. Brugger, J.; Etschmann, B.E.; Grundler, P.V.; Liu, W.; Testemale, D.; Pring, A. XAS evidence for the stability of polytellurides in hydrothermal fluids up to 599 °C, 800 bar. *Am. Mineral.* **2012**, *97*, 1519–1522. [CrossRef]
89. McFall, K.A.; Naden, J.; Roberts, S.; Baker, T.; Spratt, J.; McDonald, I. Platinum-group minerals in the Skouries Cu-Au (Pd, Pt, Te) porphyry Deposit. *Ore Geol. Rev.* **2018**, *99*, 344–364. [CrossRef]

90. Park, J.-W.; Campbell, I.H.; Malaviarachchi, S.P.; Cocker, H.; Hao, H.; Kay, S.M. Chalcophile element fertility and the formation of porphyry Cu ± Au Deposits. *Miner. Depos.* **2019**, *54*, 657–670. [CrossRef]
91. Cocker, H.A.; Valente, D.L.; Park, J.-W.; Campbell, I.H. Using platinum group elements to identify sulfide saturation in a porphyry Cu system: The El Abra porphyry Cu deposit, northern Chile. *J. Petrol.* **2015**, *56*, 2491–2514. [CrossRef]
92. Hao, H.; Campbell, I.H.; Park, J.-W.; Cooke, D.R. Platinum-group element geochemistry used to determine Cu and Au fertility in the Northparkes igneous suites, New South Wales, Australia. *Geochim. Cosmochim. Acta* **2017**, *216*, 372–392. [CrossRef]
93. Lowczak, J.N.; Campbell, I.H.; Cocker, H.; Park, J.-W.; Cooke, D.R. Platinum-group element geochemistry of the Forest Reef Volcanics, southeastern Australia: Implications for porphyry Au-Cu mineralisation. *Geochim. Cosmochim. Acta* **2018**, *220*, 385–406. [CrossRef]
94. Mungall, J.E.; Brenan, J.M. Partitioning of platinum-group elements and Au between sulfide liquid and basalt and the origins of mantle- crust fractionation of the chalcophile elements. *Geochim. Cosmochim. Acta* **2014**, *125*, 265–289. [CrossRef]
95. Crocket, J.H. PGE in fresh basalt, hydrothermal alteration products, and volcanic incrustations of Kilauea volcano, Hawaii. *Geochim. Cosmochim. Acta* **2000**, *64*, 1791–1807. [CrossRef]
96. Park, J.-W.; Campbell, I.H.; Kim, J. Abundances of platinum group elements in native sulfur condensates from the Niuatahi-Motutahi submarine volcano, Tonga rear arc: Implications for PGE mineralization in porphyry deposits. *Geochim. Cosmochim. Acta* **2016**, *174*, 236–246. [CrossRef]
97. Lui, B.; Zhang, Z.; Cheng, Z.; Xie, Q.; Turesebekov, A.; Nurtaev, B.; Santosh, M. Platinum group elements in gabbroic intrusions from the Valerianov-Beltau-Kurama arc: Implications for genesis of the Kalmakyr porphyry Cu–Au deposit. *Geol. J.* **2020**, *56*, 46–59.
98. Li, Z.X.A.; Lee, C.T.A. The constancy of upper mantle fO_2 through time inferred from V/Sc ratios in basalts. *Earth Planet. Sci. Lett.* **2004**, *228*, 483–493.
99. Toplis, M.J.; Corgne, A. An experimental study of element partitioning between magnetite, clinopyroxene and iron-bearing silicate liquids with particular emphasis on vanadium. *Contrib. Mineral. Petrol.* **2002**, *144*, 22–37. [CrossRef]
100. Williams-Jones, A.E.; Vasyukova, O.V. The economic geology of scandium, the runt of the rare earth element litter. *Econ. Geol.* **2018**, *113*, 973–988. [CrossRef]
101. Loucks, R.R. Distinctive composition of copper-ore-forming arc magmas. *Aust. J. Earth Sci.* **2014**, *61*, 5–16. [CrossRef]
102. Whalen, J.B.; Hildebrand, R.S. Trace element discrimination of arc, slab failure, and A-type granitic rocks. *Lithos* **2019**, *348*, 105179. [CrossRef]
103. Smith, M.; Kynicky, J.; Xu, C.; Song, W.; Spratt, J.; Jeffries, T.; Brtnicky, M.; Kopriva, A.; Cangelosi, D. The origin of secondary heavy rare earth element enrichment in carbonatites: Constraints from the evolution of the Huanglongpu district, China. *Lithos* **2018**, *308*, 105179. [CrossRef]
104. Cangelosi, D.; Smith, M.; David Banks, D.; Yardley, B. The role of sulfate-rich fluids in heavy rare earth enrichment at the Dashigou carbonatite deposit, Huanglongpu, China. *Mineral. Mag.* **2020**, *84*, 65–80. [CrossRef]
105. Simon, A.C.; Pettke, T.; Candela, P.A.; Piccoli, P.M.; Heinrich, C.A. Gold partitioning in melt—Vapour—Brine systems. *Geochim. Cosmochim. Acta* **2005**, *69*, 3321–3335. [CrossRef]
106. Halter, W.E.; Pettke, T.; Heinrich, C.A. The origin of Cu/Au ratios in porphyry-type ore deposits. *Science* **2002**, *296*, 1844–1846. [CrossRef] [PubMed]
107. Hill, K.C.; Kendrick, R.D.; Crowhurst, P.V.; Gow, P.A. Copper-gold mineralisation in New Guinea: Tectonics, lineaments, thermochronology and structure. *Aust. J. Earth Sci.* **2002**, *49*, 737–752. [CrossRef]
108. Heinrich, C.A.; Halter, W.E.; Landtwing, M.R.; Pettke, T. The formation of economic porphyry copper (- gold) deposits: Constraints from microanalysis of fluid and melt inclusions. *Geol. Soc. Lond. Spec. Publ.* **2005**, *248*, 247–263. [CrossRef]
109. Heinrich, C.A.; Günther, D.; Audétat, A.; Ulrich, T.; Frischknecht, R. Metal fractionation between magmatic brine and vapor, determined by microanalysis of fluid inclusions. *Geology* **1999**, *27*, 755–758. [CrossRef]
110. Pokrovski, G.S.; Borisova, A.Y.; Harrichoury, J.-C. The effect of sulfur on vapour—Liquid fractionation of metals in hydrothermal systems. *Earth Planet. Sci. Lett.* **2008**, *266*, 345–362. [CrossRef]
111. Ulrich, T.; Günther, D.; Heinrich, C.A. The evolution of a porphyry Cu–Au deposit, based on LA-ICP-MS analysis of fluid inclusions: Bajo de la Alumbrera, Argentina. *Econ. Geol.* **2001**, *96*, 1743–1774. [CrossRef]
112. Brown, A.S. (Ed.) *Porphyry Deposits of the Canadian Cordillera of North America, 15*; Canadian Institute of Mining, Metallurgy and Petroleum: Montreal, QC, Canada, 1976; p. 510.
113. Cox, D.P.; Singer, D.A. *Distribution of Gold in Porphyry Copper Deposits*; U.S. Geological Survey Open File Report; US Geological Survey: Reston, VA, USA, 1988; Open-File Report 88–46.
114. Sillitoe, R.H. Characteristics and controls of the largest porphyry copper–gold and epithermal gold deposits in the circum-Pacific region. *Aust. J. Earth Sci.* **1997**, *44*, 373–388. [CrossRef]
115. Murakami, H.; Jung Hun Seo, J.H.; Heinrich, C.A. The relation between Cu/Au ratio and formation depth of porphyry-style Cu–Au ± Mo deposits. *Miner. Depos.* **2010**, *45*, 11–21. [CrossRef]

116. Barth, M.; McDonough, W.F.; Rudnick, R.L. Tracking the budget of Nb and Ta in the continental crust. *Chem. Geol.* **2000**, *165*, 197–213. [CrossRef]
117. Kamber, B.S.; Greig, A.; Collerson, K.D. A new estimate for the composition of weathered young upper continental crust from alluvial sediments, Queensland, Australia. *Geochim. Cosmochim. Acta* **2005**, *69*, 1041–1058. [CrossRef]
118. Kamber, B.S.; Collerson, K.D. Role of 'hidden' deeply subducted slabs in mantle depletion. *Chem. Geol.* **2000**, *166*, 241–254. [CrossRef]
119. Münker, C.; Pfänder, J.A.; Weyer, S.; Büchl, A.; Kleine, T.; Mezger, K. Evolution of planetary cores and the Earth–Moon system from Nb/Ta systematics. *Science* **2003**, *301*, 84–87. [CrossRef] [PubMed]
120. Doucelance, R.; Hammouda, T.; Moreira, M.; Martins, J.C. Geo- chemical constraints on depth of origin of oceanic carbonatites: The Cape Verde case. *Geochim. Cosmochim. Acta* **2010**, *74*, 7261–7282. [CrossRef]
121. Hoernle, K.; Tilton, G.; LeBas, M.J.; Duggen, S.; Garbe-Schönberg, D. Geochemistry of oceanic carbonatites compared with continental carbonatites: Mantle recycling of oceanic crustal carbonate. *Contrib. Mineral. Petrol.* **2002**, *142*, 520–542. [CrossRef]
122. Yang, Y.; Neubauer, F.; Liu, Z.; Wang, G.-C.; Tan, S.-C.; He, X.-H.; Liang, C.-Y. Enriched lithospheric mantle storage of the Earth's missing niobium: New insights from alkaline rocks with superchondritic Nb/Ta ratios. *Geosys. Environ.* **2024**, *3*, 100289. [CrossRef]
123. Wade, J.; Wood, B.J. The Earth's 'missing' Nb may be in the core? *Nature* **2001**, *409*, 75–78. [CrossRef]
124. Perring, C.; Pollard, P.; Nunn, A. Petrogenesis of the Squirrel Hills granite and associated magnetite-rich sill and vein complex: Lightning Creek prospect, Cloncurry district, northwest Queensland. *Precambrian Res.* **2001**, *106*, 213–238. [CrossRef]
125. Mark, G. Petrogenesis of Mesoproterozoic K-rich granitoids, southern Mt Angelay igneous complex, Cloncurry district, northwest Queensland. *Aust. J. Earth Sci.* **1999**, *46*, 933–949. [CrossRef]
126. Pollard, P.J.; Mark, G.; Mitchell, L.C. Geochemistry of Post-1540 Ma Granites in the Cloncurry District, Northwest Queensland. *Econ. Geol.* **1998**, *93*, 1330–1344. [CrossRef]
127. Slack, J.F. Strata-bound Fe-Co-Cu-Au-Bi-Y-REE deposits of the Idaho Cobalt Belt: Multistage hydrothermal mineralisation in a magmatic-related iron oxide copper-gold system. *Econ. Geol.* **2012**, *107*, 1089–1113. [CrossRef]

Disclaimer/Publisher's Note: The statements, opinions and data contained in all publications are solely those of the individual author(s) and contributor(s) and not of MDPI and/or the editor(s). MDPI and/or the editor(s) disclaim responsibility for any injury to people or property resulting from any ideas, methods, instructions or products referred to in the content.